UNIVERSITY OF STRATHCLYDE

BIOMEDICAL ENGINEERING UNIT

Study of mechanical characteristics of Ankle-foot Orthoses using finite element analysis method

BY

KHANDHAR KAUSHAL PREVIN CHENDRA

This thesis is submitted in partial fulfilment of the requirements for the degree MSc in Biomedical Engineering

2014

Supervisor: Mr Stephanos Solomonidis

Copyright Statement

Signed: Date:

Acknowledgement

Special thanks to Stephanos Solomonidis for guidance throughout the whole thesis. One of the best lecturer, tutor and a person, I have ever met in my life.

Thanks to Magnus Gislason in helping me with finite element designing and modelling on Abaqus.

Thanks to Anthony Crimmin for scanning of the AFO, stitching of the scanned sections and providing me with the 3D model.

Abstract

Ankle-foot orthoses (AFOs) are external devices applied to the lower leg segment in patients with ankle joint impairment due to neuromusculoskeletal disorders resulting in abnormal gait. In the last three decades, plastic AFOs have superseded conventional metal AFOs. Prescriptions of AFOs by orthotists are usually based on trial and error and if gone wrong, cost time, money and increases the patients' rehabilitation treatment time. This is due to lack of understanding of the mechanical characteristics (i.e. stiffness) and stress distribution of AFOs. There is evidence indicating an optimal match exists between AFOs stiffness and successful rehabilitation. To date, most investigations on AFOs to determine mechanical characteristics are mechanical based. In this investigation an attempt to validate the use of finite element analyses (FEA) in order to predict stiffness and stress distribution of an AFO.

Abaqus was used to conduct FEA. The AFO model was subjected to range of loads from 100N to 700N to dorsiflex and plantarflex the AFO. The resulting analysed change in ankle angle, change in length of foot and shank segments, stress distributions were analysed.

A linear relationship was found to exist between ankle angle and moment of up to 24.9 Nm and 3.4° during dorsiflexion and moment of 23.9 Nm and 2.7° during plantarflexion and above which, non-linear behaviour is seen. FEA showed asymmetry in buckling displacements at the malleoli in medial and lateral surfaces of the AFO, where the lateral surface was found to be stiffer compared to the medial. However, this result may be inaccurate due to imprecise geometry of the AFO model. High stress concentrations were mainly around the Achilles tendon and malleoli region of the AFO during tension (plantarflexion) and compression (dorsiflexion).

It is thought that FEA may be reliable method of studying mechanical characteristics and stress distribution on AFOs but further work is needed to validate the model at its and its accuracy under various conditions of use.

Table of Content

Chapter 1: Background and Literature Review

1.1 Introduction to Ankle-foot Orthoses

The word orthosis is derived from a Greek word “ortho” which means to make straight. Orthoses not only straighten bones, but they also prevent deformities, enhance walking, assist with daily activities, alleviate pain, protect limbs, promote osteogenesis, strengthen the limbs and spine (Al Hassan, 2008)

Orthoses are devices that are applied externally to the body that serve the purpose to structurally and functionally modify neuromuscular and skeletal system attributes. Orthotic devices may be static or dynamic and may be applied to various dysfunctional body segments, such as neck, spine, arms and legs.

The nomenclature of orthotics is based on the joints that it encompasses. For example, the ankle-foot orthosis (AFO) describes an orthosis that encompasses the foot and ankle joints to a point below the knee joint (figure 1.2).

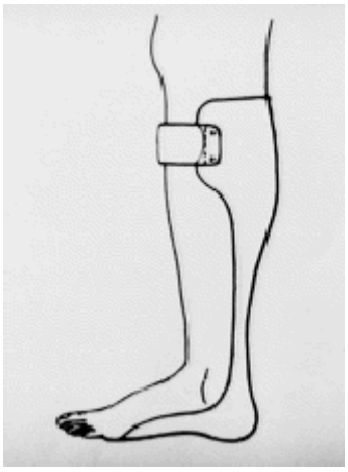

Figure 1.1: Ankle-foot orthosis (Ottobock (http://professionals.ottobockus.com) 2008)

Orthoses are aimed to correct the biomechanics of the body segments by applying forces to the body segments they encompass in order to:

i) correct deformities by re-aligning the body segment

ii) control motion of body segment

iii) compensate for absent forces due to weakened or absent muscle power

iv) alleviating pain through transferring load to another area

v) support anatomical structures from weight bearing

1.2 Clinical conditions requiring AFOs

In patients with diseases or injuries affecting the functions of neuromuscular and skeletal system which may result in abnormal joint-stabilities and muscular functions may require orthotic devices.

The following sub-chapters will describe the clinical conditions that require orthotic prescription.

1.2.1 Stroke

Stroke is an acute loss of neurological function of vascular origin with rapidly (within seconds to hours) developing clinical signs and symptoms corresponding to focal areas in the brain (World Health Organisation, 2000).

The brain, like every other organ in the body, needs adequate blood supply for its oxygen and nutrient demands to function properly. The nutrient filled-blood is transported to the brain via two main arterial systems: carotid (internal and external) and vertebral arteries. Both arterial systems are connected to in a highly branched ring shaped arterial network at the base of the brain, called the circle of Willis. The arteries branching out of the circle of Willis supplies blood to the entire brain and surrounding structures. Any occlusion or narrowing of these arteries can result into serious consequences. The disruption of cerebral blood circulation may lead to brain tissue damage or even death, and the severity of stroke is dependent on the site at which is affected within the brain and degree of hypoxia.

Strokes may be classified into ischaemic and haemorrhagic based on the condition of cerebral lesion. Ischaemic strokes may occur due to build-up of fatty plaque

(atherosclerosis), embolism, or thrombosis, which narrows and progressively occludes the blood vessel, thereby disrupting delivery of blood and inducing a hypoxic state to cells distal to the occlusion. Ischaemic strokes occur in majority of the cases and accounts up to 80% of all cases (Truelson T. et al, 2000).

Haemorrhagic strokes occur when blood vessel progressively weakens over time and is unable to withstand hydrostatic pressure of blood and bursts. This causes an injury to, not only tissues distal to the burst of blood vessel but also to surrounding cerebral tissues. Haemorrhagic strokes are often more fatal compared to ischaemic strokes due to the extent of damage.

Both types of strokes may lead to damage of the motor neurons in the brain which may cause muscle control dysfunction. Precise control and coordination of limb's flexion and extension is lost subsequent to a stroke. One of the most common signs of stroke is drop-foot, which arises due to weakness of the dorsiflexors of the foot which causes ground clearance problems during swing phase of gait. In this instance, an AFO is needed to treat this condition.

1.2.2 Motor Neuron Disorders

One of the most common reasons for AFOs treatments are loss of voluntary muscle control in patients with motor neuron disorders. This is a group of neurological disorders that destroys motor neurons which are responsible for voluntary control of muscle contraction. Motor neurons are responsible for muscle activities such as speaking, breathing, walking and swallowing.

Nerve impulses are transmitted by nerve cells from the brain to the spinal cord via the brain stem. Nerve cells in the brain to the spinal cord are called upper motor neurons and nerve cells from spinal cord to the muscles are called lower motor neurons. Upper motor neurons direct the lower motor neurons to produce movements such as walking or swallowing.

Disruptions in any nerve impulse pathway, either from upper motor neurons to lower motor neurons or lower motor neurons to muscles leads to dysfunction of muscle control and loss of stability. Depending on the site of damage and disruption of specific nerve impulse pathway and its severity, motor neuron disorders may lead to a range of symptoms, from no symptoms to paralysis or spasticity or even death. For example, damage to the lower motor neuron leads to a progressively weakening effect (paralysis) in the muscles that are innervated by the neuron. And, damage to the upper motor neuron leads to an abnormal increase in muscle tone (spasticity). Muscles that are usually commonly affected are antigravity muscles, such as hamstrings, quadriceps and adductors. These effects lead to abnormal gait which becomes stiff and slow.

Cerebral palsy is a type of motor neuron disorder, affecting the upper motor neurons in the brain. It is caused by brain damage or injury sustained during birth as a result of prenatal trauma, drug exposure or congenital defect (Martini, 2006). There are three main types of cerebral palsy: spastic, athetoid and ataxic. These types are derived from the clinical symptoms patients' exhibits. There is no cure for this disease but treatments include orthotic management to control involuntary motion, foot positioning and correct deformities.

Common clinical symptoms in these patients are *pes equinus* and *pes varus*. These signs are usually seen in patients with upper motor neuron disorders, where there is an unbalance of muscle force between the pretibial muscle groups and the plantarflexor muscles of the leg. This cause the foot to plantarflexed and medially inverted.

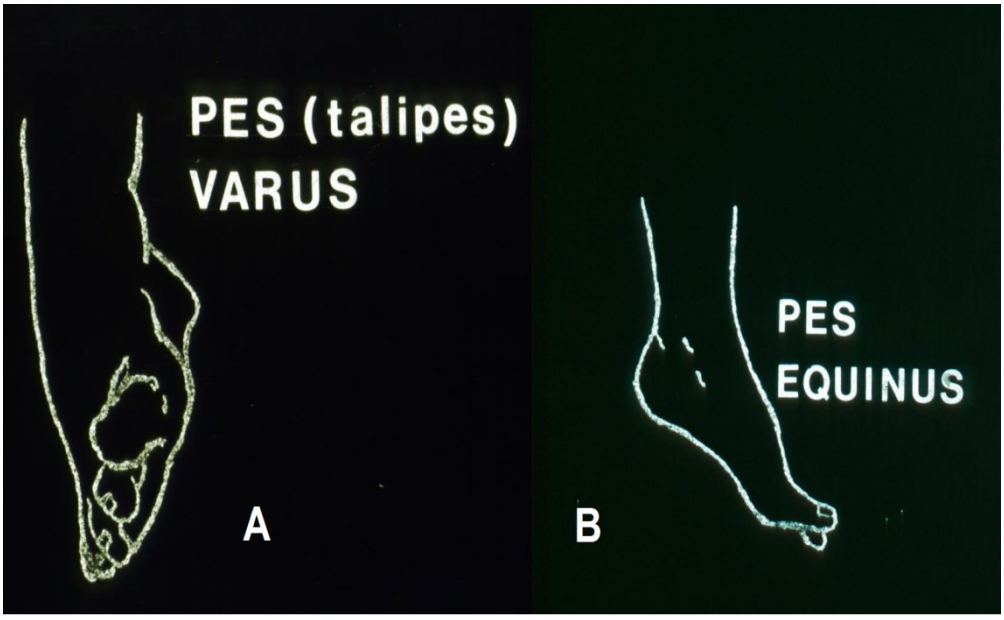

Figure 1.2 show a common clinical sign in patients with motor neuron disorders, particularly in patients with upper motor neuron lesions (Stephan Solomonidis 2007)

This deformity may be treated using rigid AFOs, which may provide a balancing moment to counter the plantarflexors and to keep the foot at plantigrade position

1.2.3 Congenital Abnormalities

Muscle dysfunction may also arise due to congenital abnormalities at birth. These abnormalities are endless, and may be present due to any developmental complication. It may be caused by genetic defects and environmental effect or a combination of the two. An example of spinal congenital disorder is spina bifida. This disease is common and is caused by an incomplete closing of the embryonic neural tube during development. This may cause damage to the spinal nerves and lead to motor dysfunctions which may require orthotics to be prescribed.

Another example of congenital abnormalities is congenital *talipes equinovarus* or club foot. This disease is caused by abnormal muscle growth which twists growing bones and joints causing foot to be rotate. Treatments include either surgery or AFO to prevent further progression of deformity.

1.2.4 Muscular Dystrophy

Muscular dystrophy is a group of muscle disease which causes progressive muscle weakness and deterioration. This is inherited and due to various gene mutation resulting in an alteration of proteins in muscles. Symptoms include poor muscular weakness, poor balance, walking difficulties, frequent falls and muscle contractures. There are no cures for these diseases but orthotics treatment may prescribe to assist locomotion.

All of these diseases/disorders lead to gait deviation from normal pattern and may cause one or more of the following:

a) Limited ankle dorsiflexion in swing phase
b) Reduced medio-lateral and anterior-posterior stability in stance phase
c) Atypical foot placement at initial contact.

All of these symptoms lead to difficulties in walking, therefore needing orthotic treatment to enhance patient's recovery and independence.

1.3 Functions of ankle, foot and associated muscles

The ankle, foot and associated muscles provide vital functions during gait:

I) Plantigrade foot position provides a strong base to support the weight of the body and it allows toe pick up during swing phase reducing chances of tripping.

II) The foot acts as body weight shock absorber during heel-strike.

III) During stance phase, foot and lower limb rotation provides an efficient directional change of centre of pressure to allow minimal muscular effort.

IV) The ankle acts as a lever during stance face and push off.

As previously discussed, in patients with clinical conditions affecting gait, the pattern of this complex would be abnormal as well. An AFO is prescribed to improve balance by maintaining anterior-posterior and medio-lateral joint ankle stability and to improve overall gait functions. As such it allows patient to walk better, faster with reduction in energy expenditure and thus allowing a near normal gait pattern (Lehmann JF, 1979).

In the next chapter we will discuss the biomechanical function of AFOs and how does it assist in patients with gait disorders.

1.4 Biomechanics of Ankle-foot Orthoses

Our bodies are constantly subjected by external forces, even when stationary, gravitational forces acts on us. In order to walk or conduct daily routines, our bodily tissues such as muscles generate large forces and moments to oppose these external forces.

As previously discussed, there is a wide range of diseases which may compromise our ability to generate opposing forces, and moments, leading to atypical gait pattern. AFOs are prescribed to compensate for inadequate internal forces to ensure gait to be relatively normal.

There are many type of designs and mechanical characteristics of AFOs, which may be specific to treat a certain disease. For example, the flaccid *pes equinus* in stroke patients is treated by a flexible AFO, whereas a spastic *pes equinus* in patients with motor neuron disease is treated with a rigid AFO. The reason being that, design and mechanical characteristics of an AFO allow manipulation of forces acting on the body, hence being disease specific.

However, all AFOs fundamentally work in similar biomechanical principle. There are five essential functions AFOs provide in order to modify internal forces and moments acting on a joint:

1. AFOs provide moments to body segments and joints to modify or redirect the rotational motion.

2. AFOs may restrict rotational joint motion. In some cases, it may be necessary to restrict motion about an axis, for example in cases where medio-lateral instability is present. It would be beneficial to restrict inversion/eversion motion of the foot, to improve joint stability.

3. AFOs may restrict translational motion at a joint. This usually occurs due to trauma to ligaments, where instead of only rotational motion, bones may also slide forward or backwards during locomotion. As such, restriction to translation motion may allow ligament healing to occur.

4. AFOs provide alternative mode of transmission of forces and moments. This function is usually due to lower limb pains, in which affected area is alleviated of any weight bearing and transferred to other anatomical structure.

5. AFOs may also provide an effective directional change in ground reaction force (GRF) axis. The realignment of GRF allows certain muscle groups to minimise muscular effort, therefore maximising efficiency.

Each biomechanical function of orthoses requires a minimum of three forces applied to specific points on patient's lower limb. These forces may be static or dynamic, and may even change in each phases of ambulation to allow better adaptation in gait.

1.5 Materials and manufacturing of Ankle-foot orthoses

There is a wide range of designs of AFO characterised by shape, material, bands and straps. An appropriate AFO prescription is mainly dependant on the nature and severity of patient's gait deficits, patient's cosmetic preferences and orthotist's recommendation. The development of new designs of AFO is predominantly due to introduction of new and improved materials in the manufacturing of AFO.

Earliest designs of AFO were mainly composed of materials such as wood, which had improved patient's gait but only marginally. In the late 1950s and early 1960s, with the introduction of stainless steel and aluminium to AFO designs, it was immediately preferred compared to wooden AFOs due to its strength, durability and adaptability, although, they are now known as conventional AFOs (Chu TM, 2001).

Conventional AFOs are distinguished by their double upright bars made of steel or aluminium alloys attached to a calf band usually made of leather and permanently fixed to a shoe. These types of AFO are also single axis designs and do not allow medio-lateral foot movement. In some conventional AFO designs, a spring or strap may be used at the ankle joint, to dampen or compensate dorsi- or plantar flexion of the foot.

Figure 1.3 shows a conventional AFO composed of metal uprights and a calf band (Advanced Orthotic Design Inc. (http://www.aodmobility.com/custom-devices/AFO/)).

However, the greatest advance in orthotic technology occurred in the 1970s, when thermoplastic materials were introduced in rehabilitation field. Since then, plastics have superseded all of the previous materials used in AFO manufacturing as they are excellent materials, can be moulded relatively easily into a wide variety shapes, and may produce a range of mechanical characteristics of AFOs. Most commonly used plastics for AFO manufacturing are polypropylene and polyethylene. They are preferred due to their material properties of high fatigue resistance, strength, light weight, effectiveness, and cost, and have better cosmesis compared to conventional AFO (Chu TM, 2001)

Plastic AFO are fabricated using a negative cast of patient's lower limb segment. Once the cast has set, it is removed and filled with plaster of Paris to obtain a positive model of the patient's lower limb segment. The positive model is then marked for bony structures and the trimlines provide optimum design for maximum orthotic fit and function.

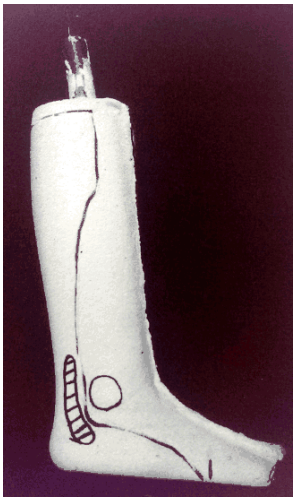

Figure 1.4 shows a patient's lower leg positive cast with trimlines on it (Stephan Solomonidis, 2007)

Then plastic sheets of orthotist's choice is draped over the positive model and cut according to the trimlines to form a custom-made AFO.

Figure 1.5 shows a variety of polypropylene AFO. The stiffness of the AFOs is decreasing from right to left. The key characteristic in order to increase stiffness is the trimline. The further anterior a trimline is, with reference to the medial malleolus position, the higher the stiffness of an AFO (Ottobock. (http://professionals.ottobockus.com))

The mechanical characteristic variability of AFO is dependent on plastic material, the thickness of the plastic sheet used, chemical composition of plastic, trimline of the AFO and geometry (Showers DC et al 1985).

Although, polypropylene may be moulded to satisfy a range of mechanical characteristics (i.e. stiffness) by the manufacture, the use of one type of plastic with certain characteristics over another is mainly determined by the orthotist's experience. This creates problems as prescriptions of AFO properties are entirely subjective to orthotists. This problem will be discussed in the next chapter.

1.6 Problem associated with prescription of AFOs

Currently, there are no gold standards in fitting and prescribing AFOs, and are largely based on qualitative assessments and dependent on orthotist's experience and judgment. The choice of a shape and stiffness of AFOs are often based on 'trial and error' (Payne et al, 2003). This is due to a lack of understanding of stress distributions and stiffness characteristics in orthoses.

This issue poses a problem as many diseases occur in a range of severity. Hence, the precise stiffness and shape of AFOs should also vary depending on the patient's disease and severity. For example patients with spasticity, where an excessive plantarflexor muscle activity generating a moment of 50 Nm, should receive a stiffer AFO compared to a patient with only 40 Nm plantarflexion moments. Also, in patients with total paralysis of their dorsiflexor muscles should receive a more flexible AFO compared to patient with mild paralysis. There is evidence indicating an optimal match exists between AFOs stiffness and patient's abnormal gait (Sumiya T et al 1996) As such, fine tuning of factors affecting stiffness is necessary to allow orthotist to select an optimum orthosis.

The current technique of 'trial and error' in fitting AFOs, leads to waste of time, material, cost and more importantly increases duration of patient rehabilitation and may have serious associated morbidity. As such it is necessary to look for convenient techniques to study stiffness and stress analysis in AFOs.

In the past decade, research in this field has been directed in quantifying mechanical characteristics of AFOs, as it is expected that these characteristics determine functions of AFOs in pathological gait.

1.7 Techniques of investigating mechanical properties and stress distribution of AFOs

Forty years ago, the prescription of AFOs predominately relied on qualitative assessments. As the issue on optimal stiffness of AFOs on individual patients has come into light in the recent past, the method of fitting and prescribing AFOs are shifting towards a more quantitative process.

Up to 1997, there were no recommended methods of determining stiffness (Miyazaki et al, 1997). In an article by Kobayashi et al (2011), strengths and weakness of many different analyses techniques were compared, to find out effective methods of investigating stiffness of AFO. In this study, Kobayashi divided all published method up to date, into (i) functional analyses and (ii) mechanical analyses.

i) Functional analyses are measurements taken which mimics a subject during ambulation. This has some obvious advantages compared to mechanical analyses that functional data takes into account physiological changes of a person during functional ambulation.

ii) In mechanical analyses, measurements are taken of AFOs during mechanical testing (i.e. without the AFO being attached to a person) of the device under forces or moments. These methods are favoured due to their reliability and accuracy in determining stiffness. Although it does not guarantee stiffness of AFO matches patient's needs.

Kobayashi then went on to provide suggestions in using data from functional analyses in mechanical testing experiments. Following are his suggestions:

a) To measure stiffness of AFOs in sagittal plane, as largest movements and many pathological disease manifestations occur (i.e. problems with dorsi- and plantarflexion of the foot) in this plane.
b) To use the physiological range of motion of ankle joint in mechanical testing experiments in various target groups. Studies on physiological range of motion of ankle had been investigated previously. In Perry et al (2010) established average range of motion to be from 10^{o} of dorsiflexion to 15^{o} of plantarflexion and Nordin et al. (2001) found range of motion of ankle varies between 10.2^{o} dorsiflexion to 14.2 plantarflexion.

In 1996, Sumiya et al. developed a simple device consisting of metal bars, a tensiometer and a protractor. With these set of devices, they found several factors affecting the stiffness of posterior leaf spring (PLS) AFOs. They found that a 3 mm thick PLS AFOs may generate a maximum resistive moment of 27.5 Nm (± 7.2 Nm) when the AFO was plantarflexed by 15^{o}. Although this simple device is a good estimator of stiffness of an AFO, the variability (i.e. standard deviation) of this method is high and lacks capabilities of precise and accurate measurements.

In 2004, Major et al. investigated moments and dorsiflexion foot angles about the malleoli on AFOs with several forward trimlines using an Instron machine. They measured the change in lengths of proximal to distal loading points to calculate the dorsiflexion angle, using the cosine rule equation (see figure 1.6). In their calculations, they assumed lengths of

shank and foot. This study investigates on four types of AFOs and their loading patterns in ten loading cycles.

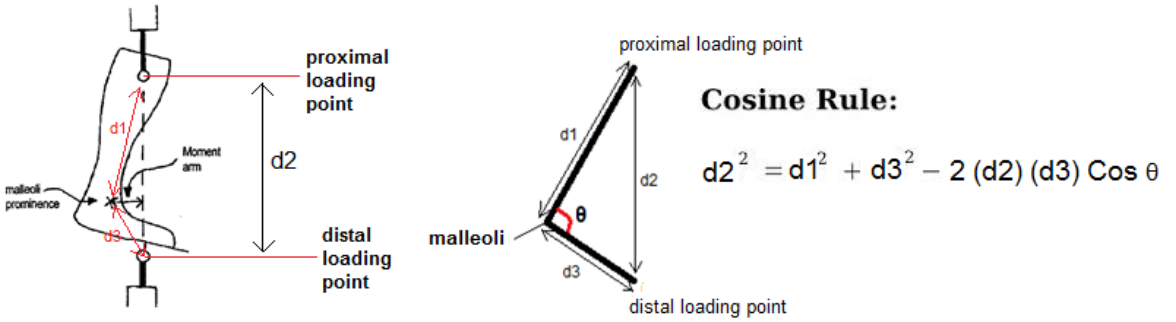

Figure 1.6 shows an AFO mounted in an Instron machine showing the orientation of the moment arm, loading points and lengths of d1, d2, d3 based on Major's investigation. They measured the length of proximal to distal loading point and calculated the ankle angle using the cosine rule. They assumed lengths of d1 and d3 to be constant throughout their calculation. (Major et al. 2004).

It was found that the co-polymer polypropylene AFO used by them showed linear behaviour up to 10 Nm, and thereafter, showed non-linear material behaviour. There is a large moment difference in comparison to values found by Sumiya et al. (1996) and Yamamoto et al. (1993). This is likely to be due to the chemical composition of the polypropylene material in the AFO. Although the this test is accurate and precise in determining stiffness of AFOs, it is likely that AFOs being tested undergo change in material properties when subjected to high loads.

Over many years, Chu et al. (1996, 1998, 2000, and 2001) experimentally investigated stiffness and stress distribution of AFOs and their relationships using strain gauge technology. Results from investigation (Chu et al. 1998) showed peak stress concentrations occur primarily in the Achilles tendon regions of AFOs but changes with orthoses geometry, and rigidity. It was found that strain gauge technology is an excellent technique with high accuracy in determine stiffness and stress distributions of AFOs, although the accuracy highly depends on the specific bonding techniques of strain gauge to material surface. The stiffness of AFOs was shown to increase when materials was tested with UV-treated bonding in comparison to non-UV-treated bonding techniques (Chu et al. 1996, Enrica Papi.2012), although no standard bonding procedure has introduced, as such results may not be comparable.

Bregman et al. (2009) developed a new device for evaluating AFO characteristics named BRUCE. This device evaluates the AFO stiffness and neutral angles around the ankle and metatarsal-phalangeal (MTP) joint and is based on an AFO mounted on a dummy leg with anatomical based centre. The device works by manually deforming an AFO which allows flexion-extension around the ankle and MTP joint. BRUCE was shown to have a high reliability and precision with errors in stiffness value of less than 4%. Furthermore, the device does not require a trained person to operate it.

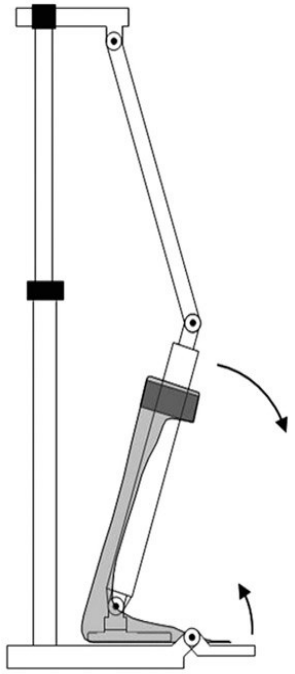

Figure 1.7 shows the schematic design of BRUCE. The arrows indicate the direction of moments to allow ankle dorsi-plantarflexion motion and flexion-extension of the foot joint (Bregman et al 2008).

The main limitations were the accuracy of the measurements and feasibility and the fact that the movement/force applied to the experimental AFO may not mimic the loading during gait (Papi 2012).

As all previous mechanical testing methods discussed are based on mechanical tests on existing AFOs, which may involve high costs (i.e. to construct a custom-made AFO) and

excessive time to conduct accurate and reliable experiments. Additionally, the AFOs may also undergo specific permanent deformation if tested repeatedly which may lead to unreliable results. As such, it is necessary to look at computational methods of studying AFOs.

One method of computational investigation on mechanical properties and stress distributions of AFOs theoretically is using finite element analyses.

1.8 Introduction to Finite Element Analysis

Finite element analysis (FEA) is a computational technique which predicts how structures behave in upon subjected to “real-world” forces, vibration, heat, and other physical effects. FEA is traditionally a branch of solid mechanics which uses numerical analyses of various complex engineering and multiphysics structural problems, although it has evolved to incorporate fluids and fluid dynamics as well. It is particularly useful for complicated geometries, loading and material properties where analytical solutions may not be obtained or feasible in a real-world experiment.

There are many computer softwares which are able to solve FEA such as ANSYS, PATRAN, Abaqus and others. All of these softwares conduct their analyses by subgrouping constituents of a structure, namely geometry model, material properties of elements, loads and boundary conditions.

a) Geometry models: This involves designing of structures with correct representation of dimensions in the software. The design of structures may be built on the software or may be imported via a scanning device (i.e. computerised tomography scan or three-dimensional laser scan). The geometry model is then meshed to divide it into elements and nodes. Each element are analysed individually and collectively summed in a global system to allow an accurate simulation to take place. A higher count of elements and nodes will result into a more accurate and detailed analyses, though, it will also increase the model complexity and the duration of numerical calculation.
b) Material properties of elements: This involves correctly inserting material properties of all elements of the model. This may include Young’s modulus (E), Poisson’s ratio

(*v*) for elastic materials and further values of yield stress, plastic strain, and strain-rates for plastic materials. And, depending on the material property defined, appropriate values of constants are necessary to be specified. This enables the software to accurately analyse a structure based on the values of constants inserted to simulate and represent a real-world simulation.

c) Loads: This section involves assigning loads at specific surfaces or nodal points on the model. The loads may be in the form of forces, moments, torques, stresses, pressure, vibrations, heat or other physical effects. These loads may be also specific in a various ways, for example, concentrated point load, uniform load and others. Furthermore, in models with two or more materials; we may also specify how all of the materials react with each other, by specifying interaction between them. This interaction dictates how the materials behave when in contact with another material.

d) Boundary conditions: Boundary conditions are specified values of field variables on the geometrical model. For example, if a beam is fixed (i.e. fixed with respect to X, Y and Z-axis) at one end, it would be necessary to specify a boundary condition of zero displacement at that point. This would allow the FEA software to form mathematical equations which would be needed to solve the analyses.

Based on all of the data input on geometrical model, material properties, loads, and boundary conditions to the FEA software, it would analyse and solve equations to achieve an approximate solution.

Upon reaching a solution, all FEA software allow users to use visualise on a variety of parameters of the model, for example stress analysis, heat transfer, fluid transfer,

electromagnetic change and others. This function is called the post-processor. The post-processor function also allows users to retrieve plotted graphs and diagrams of variety of parameters as above; this allows fast and efficient data collection.

1.9 Previous studies on Finite element analysis on AFOs

Researchers have begun conducting FEA on AFOs in the mid-1980s, although preliminary studies were conducted in very simplistic models. Leone et al (1987, 1988, and 1991) developed a mathematical model of an AFO using beam equations and small deflection theory. Reddy et al. (1985) and Lam et al. (1987) developed a two-dimensional symmetrical model of the AFO complex. The results from these studies concluded that peak stresses occur in Achilles tendon and heel region of the AFO. Although it shows some viability of early models in simulating real life mechanical tests, but in real life, AFOs are not symmetrical and may not be treated as a two-dimensional model.

Chu et al. (1995) formulated a three-dimensional finite element model of an asymmetrical AFO together with the foot (i.e. including ligaments, bones and soft tissues). The Young's modulus (E) of each material type was used individually assigned and are 11.5 MPa, 14000 MPa, 1.15 MPa, and 1030 MPa for ligaments, bones, soft tissues and orthosis respectively. And, the Poisson's ratio of 0.35, 0.49 and 0.43 for bones, soft tissue and orthosis respectively. This study revealed that peak stresses occurred in the Achilles tendon and heel region, corresponding to tensile stress and compressive stress respectively during toe-off. As this investigation was the first to model an asymmetrical AFO, it was also revealed that there are significant variations between the medial and lateral sides during swing phases of gait. This model gives us a clearer picture of the stress distributions in AFO in a normal person but Chu failed to take in to consideration non-linear material properties of soft tissue, bones, ligaments and polypropylene as all of the materials were assumed to be linear, perfectly elastic and isotropic and ignores large deformations. As such, values peak stresses may be unreliable, although it must be noted, regions of high concentrations (i.e.

Achilles tendon and heel regions) is supported Chu et al. (1996) using strain gauge technology as well.

In 2004, Syngellakis et al. improved on previous work of Chu et al. (1995) by developing a finite element model of a symmetrical model of posterior leaf AFO. This model is based on real material properties of co-polymer polypropylene, which is a multilinear material. Syngellakis specified uniform thickness of 2 mm and initial Young's modulus (E) as 1390 MPa, with decreasing stiffness above stress of 13 MPa. The Poisson's ratio (v) adopted was 0.35, although he noted, that AFO response did not change significantly with any value of v between 0.35 to 0.45. Syngellakis subsequently applied a series of simulation tests designed to investigate relations between AFO trimline location and stiffness for moderate and large rotations. Syngellakis concluded that their investigation suggests FEA on AFOs is reliable and effective in assessing behaviour of AFOs. However, no comparison with data from mechanical testing on existing AFOs with identical material properties was done.

1.10 Study aims

In this investigation an attempt will be made develop a three-dimensional finite element model of a polypropylene AFO, in order to predict the mechanical characteristics and stress distributions under simulation of an AFO in an Instron machine. The following characteristics of AFOs are studied:

a) The stiffness of AFO by evaluating foot rotations of an AFO under loading and appropriate boundary conditions to simulate a tensile test in an Instron machine
b) The buckling characteristics of AFO under dorsiflexion loading.
c) Stress distribution under load

The following results will be compared to data of mechanical tests on identical AFOs to validate the reliability and feasibility of FEA. We hypothesis FEA once validated will be able to predict the stiffness and stress distributions of AFOs.

Chapter 2: Methodology

This chapter will introduce three-dimensional scanning and finite element analysis and explain in detail the methodology and procedure in conducting the experiment with regard to geometry scanning, modelling, specification of material properties and data collection.

2.1 Introduction to three-dimensional scanning

The innovation of three-dimensional scanning has been a tremendous advancement in the field of design engineering. Many structures with complicated geometries are being able to be digitalised or computer modelled with high accuracy and precision. This in turn has allowed many computer-aided analyses of these structures to be easier and faster.

There are many types of scanners, which captures the dimensions of objects by using lasers, lights, and x-rays. These utilise various and different principles of imaging, but the two most common ways in capturing geometry of an object is the short-range and long-range scanning methods.

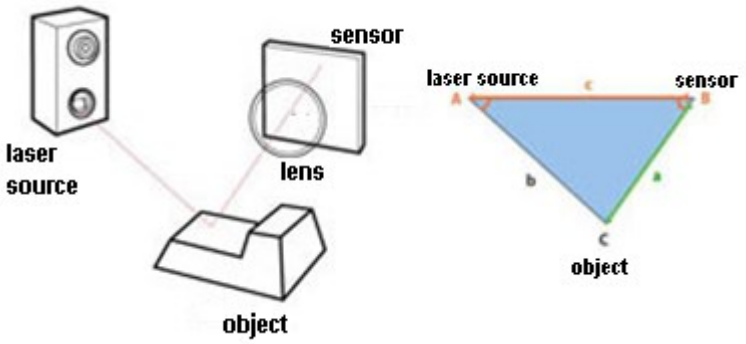

Figure 2.1 shows the principle of short-ranged imaging technique adopted by many three-dimensional scanners. This type of scanners uses the trigonometric triangulation (on the right) where the distance and angles between laser source and sensors are known. (3D System Inc. Geomagic (http://www.rapidform.com/3d-scanners/))

a) Short-range scanning principle: Short-range laser scanners use laser triangulation technique, where a single (or many) laser point to scan across an object at a distance of not further than one meter. The laser source is directed to an object of interest and reflection of the laser is picked up by a sensor. The distance and the angle between the laser source and sensors are known, and using trigonometric triangulation, the system calculates the distance between object and laser source and object and sensor; hence geometry of the object is determined.

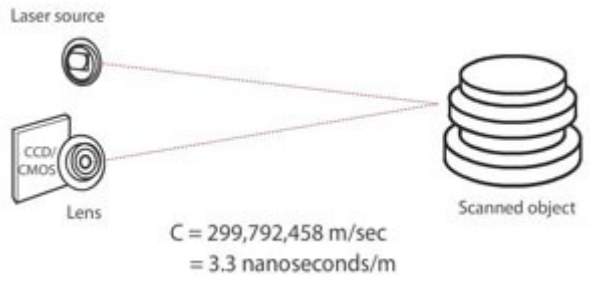

Figure 2.2 shows a common principle of imaging of a three-dimensional long-range scanner. This type of scanner uses the change of laser speed and time taken for the reflected laser to be reflected by the object and captured by the sensors. (3D System Inc. Geomagic (http://www.rapidform.com/3d-scanners/))

b) Long-range scanning principle: In contrast to short-range scanners which use distance and angles, long-range scanners usually us the principle of change in laser speeds and time. The speed of laser is precisely known, as such when directed to an object and reflected to a sensor, the system calculates the change in laser speed to computer the geometry of an object of interest. The system is very accurate, usually measures the time to picoseconds. This allows accurate calculation of distance and geometry of the object as well.

The use of one scanner over the other is usually based on cost, availability and appropriateness. For this experiment we use the short-range laser three-dimensional digitizer, KONICA MINOLTA VIVID 9i model.

2.2 Background of existing AFO

The existing AFO in our investigation was custom made from a volunteer's left foot, and by homo-polymer polypropylene. The dimensions of the AFO are illustrated in the figure below.

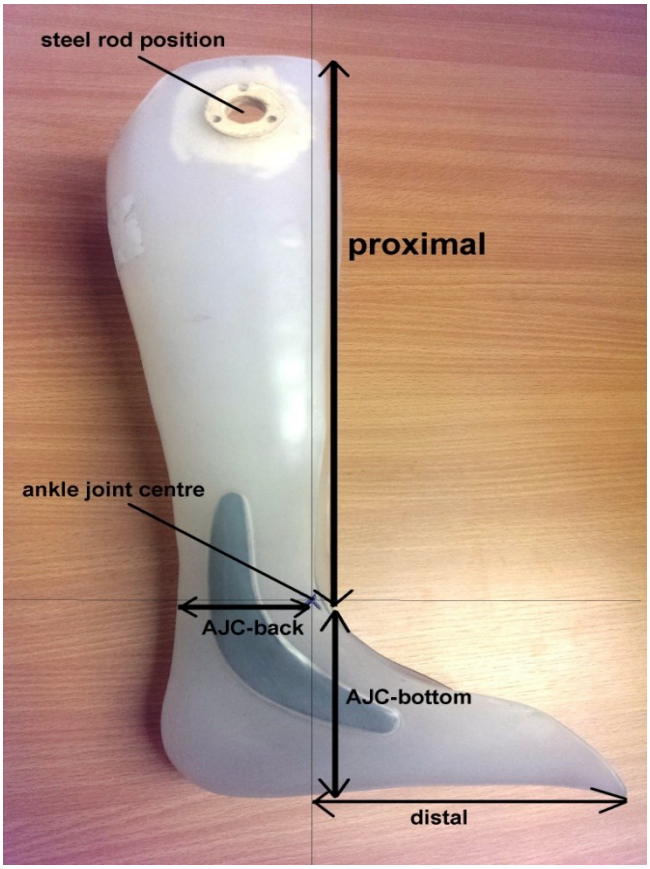

Figure 2.3 shows the AFO with parameters defining its geometry with the position of ankle joint centre (AJC) and position of steel rod labelled. Dimensions are proximal = 252 mm, distal = 119 mm, AJC is located 95 mm from the bottom and 52 mm from the back.

The trimline is located 4 mm anterior to the AJC; as such the stiffness of the material is likely to be high, making the AFO rigid. In a tensile test (i.e. using Instron machine), a steel rod is fixed at the position labelled in the figure above, which is 35 mm from the top and 72 mm from the back. The steel rod holds the AFO firmly while a force is subjected from the foot in the direction to the steel rod. In our experiment, we try to simulate the behaviour of the AFO in an Instron machine using computer-aided finite element analysis.

2.3 AFO geometry model scanning

All surfaces AFO was uniformly sprayed with a quick drying liquid spray of finely divided white powder (ARDROX 9B1D, Chemetall Ltd, Germany) and left for few minutes. The spray is used to minimise any reflection of laser away from the sensor.

A short-range three-dimensional scanner, the Kinoca Minolta VIVID 9i (Kinoca Minolta Ltd, UK) is used in order to scan the AFO. The setup of the scanner is shown below. The scanner box includes a laser source (at the top) and a sensor and lens (at the bottom) at an angle.

Figure 2.4 shows Kinoca Minolta Vivid 9i (on the left), the assembly of the scanner (middle) and the rotating stage (on the right). The scanner was set up on a tripod facing the AFO at a distance of 1m. The AFO was placed on the rotating stage, fixed upright by blue tacks.

Once the setup is completed, the coated AFO is fixed upright on the rotating stage by blue tacks in order to stop any AFO motion with respect to the stage, which reduces error in scanning process to produce better digital image. The scanner took a total of four scans, from top to bottom in a plane. After one plane has been scanned, the stage rotates 120˚ and scanning continues. This occurs three times to take a complete 360˚ image of the AFO.

The digital images scanned are transferred to the computer in four layers (i.e. one from every plane) in Geomagic Studio 9 (Geomagic Solution Ltd, USA) software. Geomagic is used to stitch all images from four planes to form a three-dimensional image. The image of AFO was in the format of a drawing (.dxf file), as such was imported to Solidworks (version 2013, Dassault Systemes Ltd, France) and converted to a three-dimensional geometry model (.iges file). This step is necessary as Abaqus do not recognise .dxf files.

2.4 AFO geometry model design and meshing

The scanned AFO three-dimensional geometry model (IGES file) was imported in Abaqus (version 6.12-3, Dassault Systemes, France). The relative complexity of model in terms of curvature and presence of rough edges and gaps or holes forced us to manually re-surface four gaps and smooth out presence of rough edge especially at the curvatures. This step was necessary in order to validate the geometrical model in Abaqus.

To simulate an AFO in compression and tension on Instron machine, we added a steel rod geometrical model (of diameter = 11.2 mm and length = 110 mm) into the AFO model. The steel rod was tied (attached and constrained) to the lateral interior surface of the AFO at 35mm from top, and 72 mm from the back of AFO model.

Due to the relative thinness (thickness of 4.6 mm) of the AFO model in comparison with other dimensions and surfaces, it was thought a three-node triangular homogenous shell element option in Abaqus was appropriate in defining AFO element type. Whereas, for the steel rod, it was thought the six-node hexagonal homogenous solid element type was appropriate. The geometrical model element types also have six degrees of freedom (three translations and three rotations) per node and this allows deformation to occur in any mode and direction in three-dimensional space.

The finite element model of AFO shell and solid steel rod was automatically meshed separately. All settings and parameters of meshing was set at default to form a shell element (i.e. AFO) of 5586 shells, 10457 edges, 4867 vertices and 52049 elements, and solid element (i.e. rod) of 1 cell, 2 edges, 2 vertices and 8016 elements.

The thickness of the AFO shell was set to be at 4.6 mm, although it has been reported to be non-uniform and varies between positions on the AFO. It was reported that all plastic AFO may have some degree of variance in thickness of AFO, for example the thickness located at the heel region was approximately 50% of maximum thickness of AFO, and average thickness at the ankle trimline was approximately 80% of maximum thickness of AFO. In this simulation we assumed uniform and constant thickness of 4.6 mm throughout the AFO model.

2.5 Material properties and parameters of AFO

a) Ankle-foot orthosis model: At operating temperature, polymers such as polypropylene behave as a non-linear material, with decreasing of stiffness at higher stresses. As such careful considerations need taken into specifying material properties and parameters of the AFO model. From previous tensile test studies by Papi at the University of Strathclyde Bioengineering Unit, UK, on an identical AFO, it was found that the mean Young's modulus, E was 1900 MPa, which is the value we used in our AFO finite element model (Papi, 2012). This value is significantly larger than values of E in literature on polypropylene AFOs which states between 1000 – 1400 MPa. This was due to the particular type of polypropylene material used in our AFO. Most literature review had used, co-polymer, whereas we used homo-polymer type polypropylene. The literature does not suggest any distinction between the two types, although we had previously found homo-polymer polypropylene to be significantly stiffer material compared to the other.

Most plastic have a Poisson's ratio, (v) of between 0.35 0 - 0.45, we adopted the value of 0.42 in our AFO model (Papi 2008). The value of v is not critical, as materials remained unchanged upon variation of v. (Syngellakis et al, 2004)

As polypropylene is non-linear elastic material, we took into consideration of plastic deformation induced in increasing loads; the yield stress and plastic strain were specified in Abaqus as follows:

Yield Stress (MPa)	Plastic Strain
2	0
7	0.001
15	0.002
20	0.0038
25	0.0052
30	0.006

Table 1: shows values of yield stress and plastic strain specified in Abaqus, the values have been taken from a study conducted by Papi on an identical AFO (Papi 2012).

b) Rod model: The rod was assigned to properties of steel, where we specified an elastic material with E = 200 GPa and v = 0.25.

2.6 Load and boundary condition specification

The AFO model was rotated 20.9° clockwise, to align the steel rod and the middle of the front edge of AFO along the Y-axis (the line of axis of loads). This step was taken, in order to allow equal and opposite loads and in the same line of axis to be subjected at steel rod and the foot and to minimise any unwanted moments in other axis. The value of 20.9° was calculated by trigonometric equations using the dimensions of the AFO.

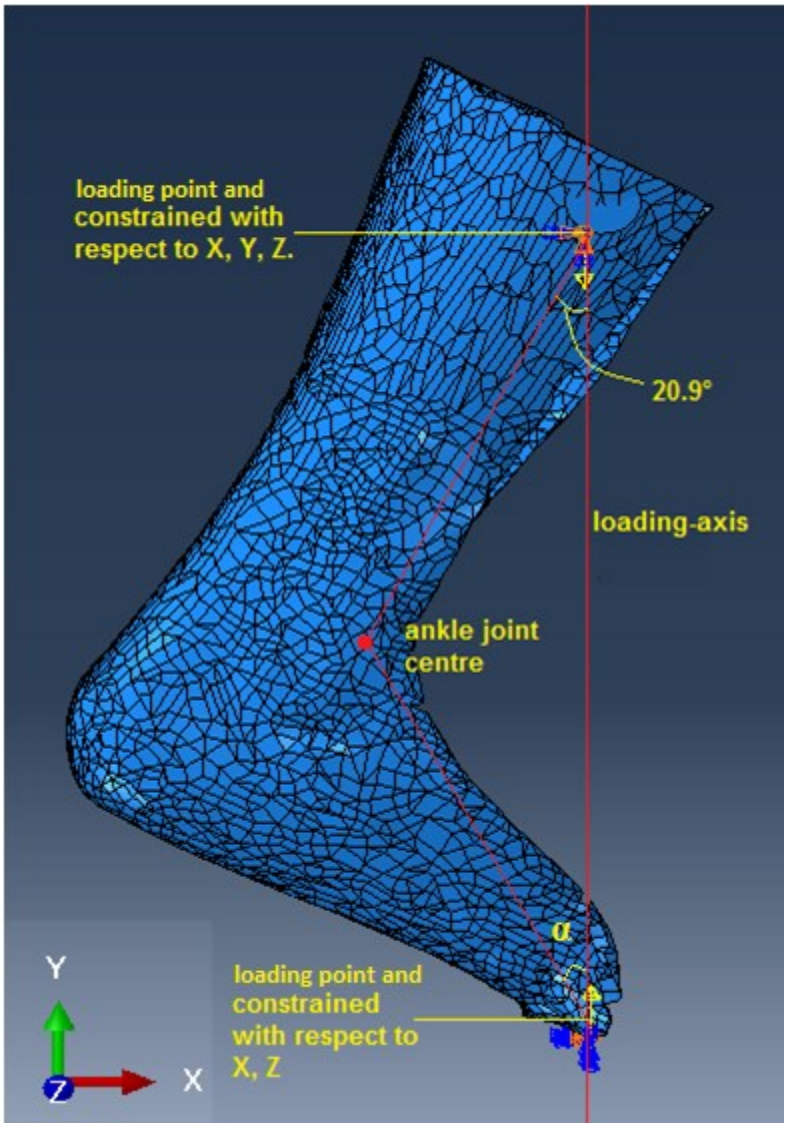

Figure 2.5 shows the finite element model of an AFO with loading and boundary conditions. The AFO is rotated by 20.9 degrees to mimic loading conditions in of an AFO in an Instron machine.

$$\tan(90-\alpha) = \frac{distance\ of\ steel\ rod\ position\ to\ bottom}{distal\ distance}$$

$$= \frac{(\ Proximal\ ) + (\ AJC\ to\ bottom\ ) - (\ distance\ of\ steel\ rod\ position\ from\ top\ )}{distal\ distance}$$

$$\tan(90-\alpha) = \frac{252+95-35}{119}$$

$$90-\alpha = 69.1°$$

$$\alpha = 20.9\,°$$

Finally, the finite element model of AFO and rod was subjected to specific loads and boundary condition as follows:

a) Loads: A 102 nodes set were created, at the middle of the front edge (as shown on figure 2.5) of the AFO; these nodes were subjected at uniform load, collectively at +100 N, +200 N, +300 N, +400 N, +500 N, +600 N and +700 N in Y-axis for dorsiflexion and collectively at -100 N, -200 N, -300 N, -400 N, -500 N, -600 N and -700 N in Y-axis for plantarflexion.

   A set of 4 nodes had been created, 2 nodes on each surface end of the steel rod (as shown on figure 2.5); these nodes were subjected at of uniform equal magnitude but in the opposite direction to the ones above. To measure dorsiflexion, we used -100 N, -200 N, -300 N, -400 N, -500 N, -600 N and -700 N in Y-axis and for plantarflexion, we used +100 N, +200 N, +300 N, +400 N, +500 N, +600 N and +700 N.

b) Boundary conditions: On the nodes previously discussed, we specify zero displacement in X, Y and Z-axis on the 4 nodes on the steel rod model and zero displacement in X and Z-axis but free to move in the direction of Y-axis on the 102 nodes on the foot. This allows dorsiflexion and plantarflexion of the AFO about the

ankle joint centre (rotation centre) but not rotation caused by moments in x- and y-direction.

2.7 Data collection

Upon solving of the FEA, the post-processor function is used in order to collect data of rotation about ankle joint (i.e. dorsiflexion and plantarflexion), moments and stresses.

a) Ankle joint rotation: The ankle angles was calculated by retrieving the coordinates of three nodal points on the AFO model; this enabled us, to calculate the angle between them, before and after deformation using the cosine rule equation of angle between two vectors, to allow us to calculate the change in ankle angle (δθ) of the foot (sample calculation is shown in appendix).

$\boldsymbol{a} \,.\, \boldsymbol{b} = |\,\boldsymbol{a}\,|\,|\,\boldsymbol{b}\,|\,\cos\boldsymbol{\theta}$ **, where a = position vector of A (node 23338) with respect to B (node 9868) , where b = position vector of C (node 16185) with respect to B and θ = angle of ABC.**

The three nodes chosen are node 23338, 9868, and 16185 and their locations are in the figure below.

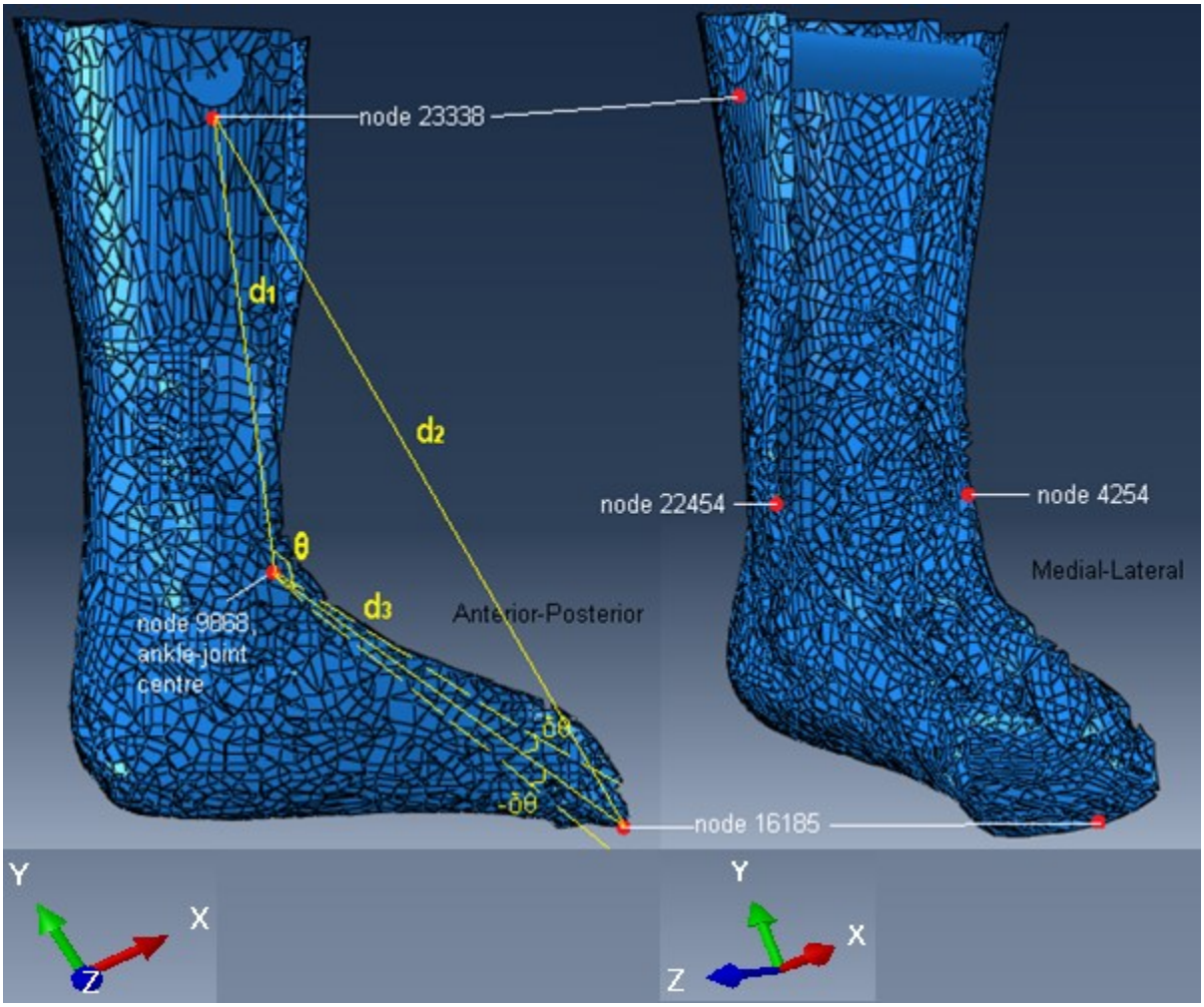

Figure 2.6 shows the AFO model with the anterior-posterior and medial-lateral view of the AFO model, with labelled nodal points used in order to calculate the change in ankle angle (dorsiflexion or plantarflexion of the foot) and displacements. The nodal point 23338 is at the lateral surface of the AFO (just below the steel rod), nodal point 9868 is at the medial malleolus or ankle joint centre, nodal point 16185 is at the middle of the front foot edge of the AFO, nodal point 22454 and 4254 is at the medial and lateral curvature of the AFO as show in figure. Figure above also shows displacements of d1 (node 23338 – node 9868, d2 node 23338 – node 16185, and d3 (node 9868 – node 16185).

The nodal point locations were chosen based on boundary conditions and location of the ankle joint rotation centre (medial malleolus). The location of nodal point 23338 is not entirely crucial and just acts as a reference point but the other two are. The nodal point 9868 was chosen based on the location of rotation centre of the real AFO. This point was measured to be 95 mm from the bottom heel surface, and 52 mm from the posterior surface of the AFO. These distances were translated into the AFO model, to achieve the precise location of nodal point 9868. Whereas the nodal point 16185, was chosen based on

the boundary conditions and location of the load at the foot which ensured only change in Y-coordinates (as the nodal point is fixed with respect to X- and Z-axis), which we were interested in.

The initial angle ($\theta_{initial}$) and the final (deformed) angle (θ_{final}) were used to calculate the change in ankle angle ($\delta\theta$).

$$\theta_{initial} - \theta_{final} = \delta\theta$$

b) Moments: The moments were calculated using the function of creating a new axis in Abaqus. Two lines were created; one was from the medial-front edge of the food (at the location of loads) to vertically upwards to the at the steel rod (medial-bottom surface) and another line from nodal point 9868 (ankle rotation centre) to an intersecting point at the first line (the second line was ensured to be perpendicular in X-Y plane to the first line).

   The moment was calculated by using the distance (i.e. distance in X-Y plane) from nodal point 9868 to the intersection point of the first line, and multiplying with the load used.

c) Change in lengths: Change in lengths of d1 (nodal point 23338 – 9868), d2 (nodal point 23338 – 16185), d3 (nodal point 9868- 16185) is calculated in two-dimensions (i.e. changes lengths with respect to X- and Y-axis)

d) Displacement: Additionally, we further defined two nodes (nodal point 22454 and 4254) as seen in figure 2.5, to calculate the buckling displacements during dorsiflexion. Only lateral displacements (i.e. displacements in Z-axis) were

considered in calculation of buckling displacements. These points were chosen due to visually showing highest lateral displacements and stresses.

e) Stresses: The stresses were available directly from the post-processor visualisation function of Abaqus.

Chapter 3: Results

3.1 AFO stiffness

The overall analysis of the finite element model of AFO showed variability in material behaviour dependant on loading. It was found that when a dorsiflexion moment was applied the AFO behaved linearly only up to 24.8Nm and change in ankle angle of 3.4^{o}; with further increasing in load, the AFO behaves non-linearly (figure 3.1). On the other hand, during plantarflexion, AFO behaved linearly up to 23.9 Nm but with a lower change in angle of -2.7^{o} (figure 3.2). This shows that the AFO model demonstrates greater resistance during plantarflexion compared to dorsiflexion.

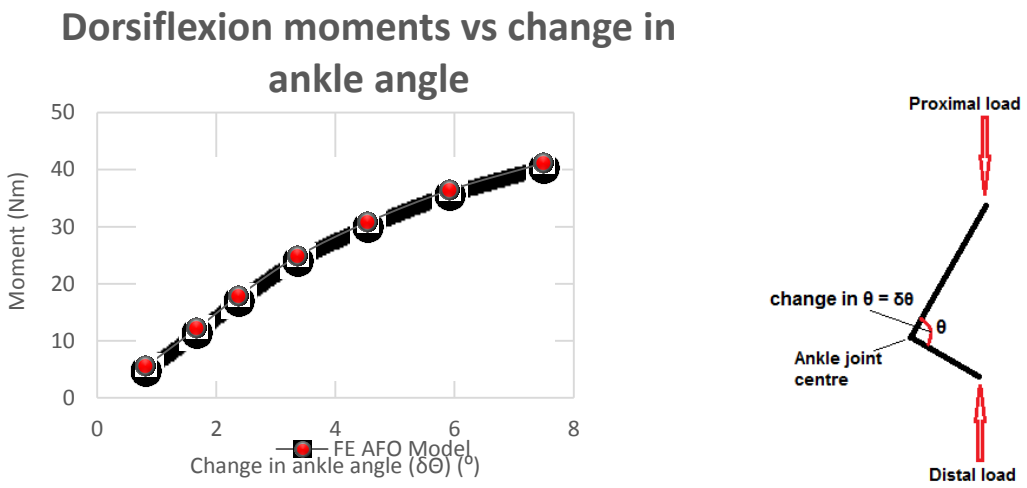

Figure 3.1 shows a graph of moments vs change in ankle angle of the AFO model during dorsiflexion, and a simplistic line diagram to represent the AFO with direction of loading and ankle angle corresponding to the graph. The AFO behaved linearly with increasing moment up to 24.8Nm and change of ankle angle of 3.4°, and further increase in load showed decreasing stiffness.

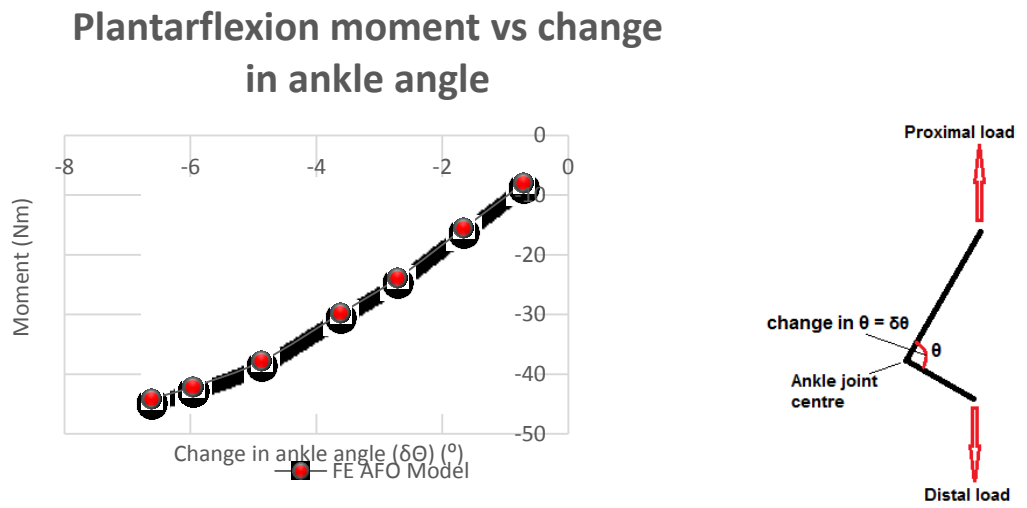

Figure 3.2 shows a graph of moments against change in ankle angle of the AFO model during plantarflexion, and a simplistic line diagram to represent the AFO with direction of loading and ankle angle corresponding to the graph. The AFO behaved linearly up to -23.9Nm and change of ankle angle of -2.7°, and further increase in load showed decreasing stiffness.

3.2 Buckling stresses and displacement affected by model symmetry

It is commonly known that under dorsiflexion, an AFO may buckle. To investigate this phenomenon, we looked at the malleoli points of the AFO to study the relationship between the stresses at the buckling region (in this thesis, it is referred to as buckling stress) and lateral displacements (with respect to Z-axis). We defined two nodal points 22454 (medial) and 4254 (lateral) (shown in figure 2.6) and comparing with stresses at their location. These two points were chosen as maximum displacement was seen to occur at these points.

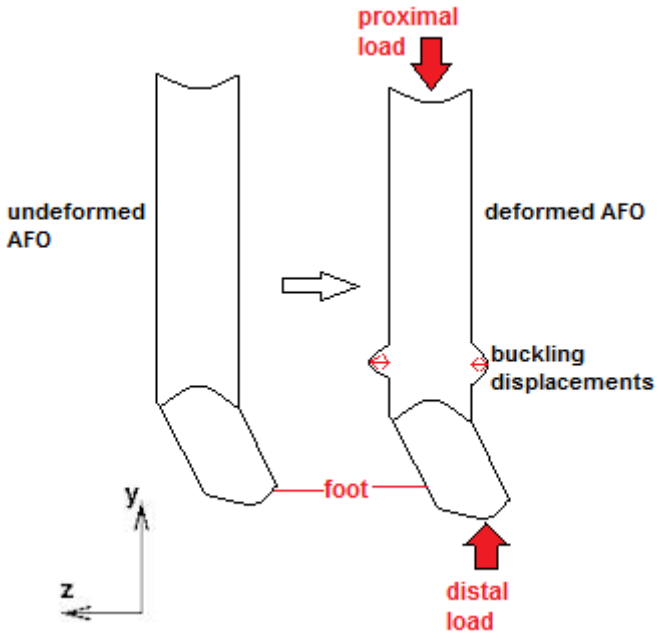

Figure 3.3 shows a simplistic figure of undeformed and deformed AFO during dorsiflexion. The buckling stresses are obtained at the nodal points 22454 (medial surface) and 4253 (lateral surface). The buckling displacements are defined in the diagram.

The medial surface of the AFO was found to yield at 29.6 MPa and lateral displacement of 9.2 mm. This is shown by the decrease of stress with further displacements above 29.6 MPa.

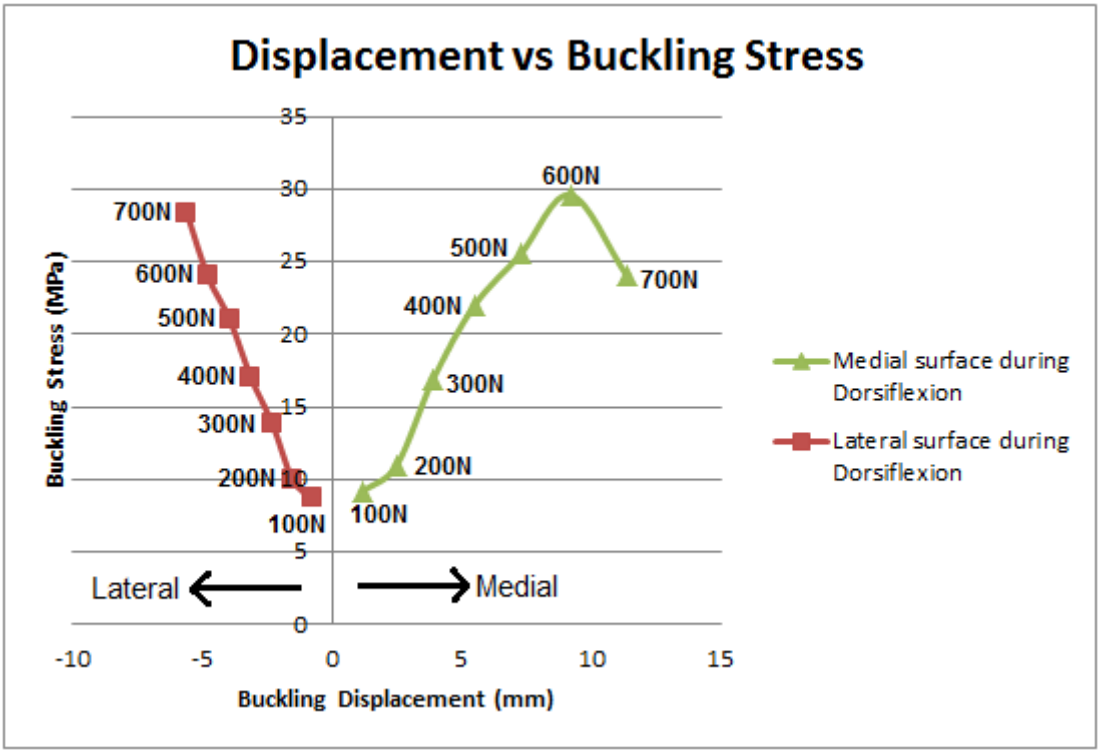

Figure 3.4 shows stresses against buckling displacement (i.e. lateral displacement) at medial and lateral nodal point (i.e. nodal point 22454 and 4254 (see figure 2.6)) of the AFO. Loads at all points are specified in the graph.

In comparison, the lateral surface did not yield at buckling stress of 28.3 MPa and lateral displacement of 5.6mm (see figure 3.4). Forces produces higher stresses in the medial surface during dorsiflexion compared to lateral surface of the AFO finite element model (see figure 3.4). The asymmetry in the stress distribution was also found in Chu et al (1995), this was thought to be due to asymmetrical nature of geometry of the AFO.

3.3 Change in lengths of d1, d2, d3 against the loads applied

In a previous study by Major et al (2004), they assumed lengths d1 and d3 to remain constant under loading throughout all of their calculations. This we thought may be an oversimplification of AFO response, and in order to investigate their assumption we collected data of changes of these parameters against corresponding forces.

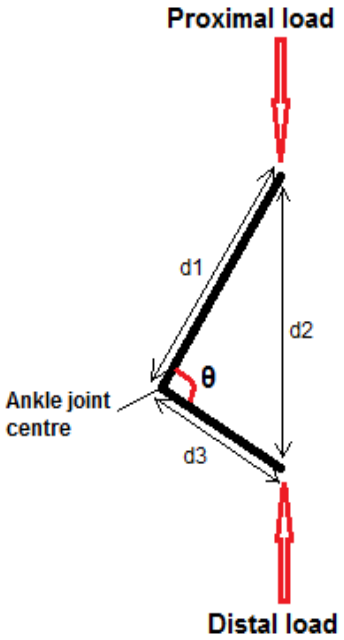

Figure 3.5 shows a simplistic line diagram representing an AFO which specifies the loading direction in dorsiflexion and lengths of d1, d2, d3.

Change of length of d1, d2 and d3 are calculated using changes in lengths of nodal point 23338 to 9868 (d1), 23338 to 16185 (d2) and 9868 to 16185 (d3) between deformed and undeformed condition of AFO (figure 2.6). We calculated the magnitude of changes of respective lengths in X- and Y-axis (i.e. two dimensional) and plotted values against corresponding loading (figure 3.6).

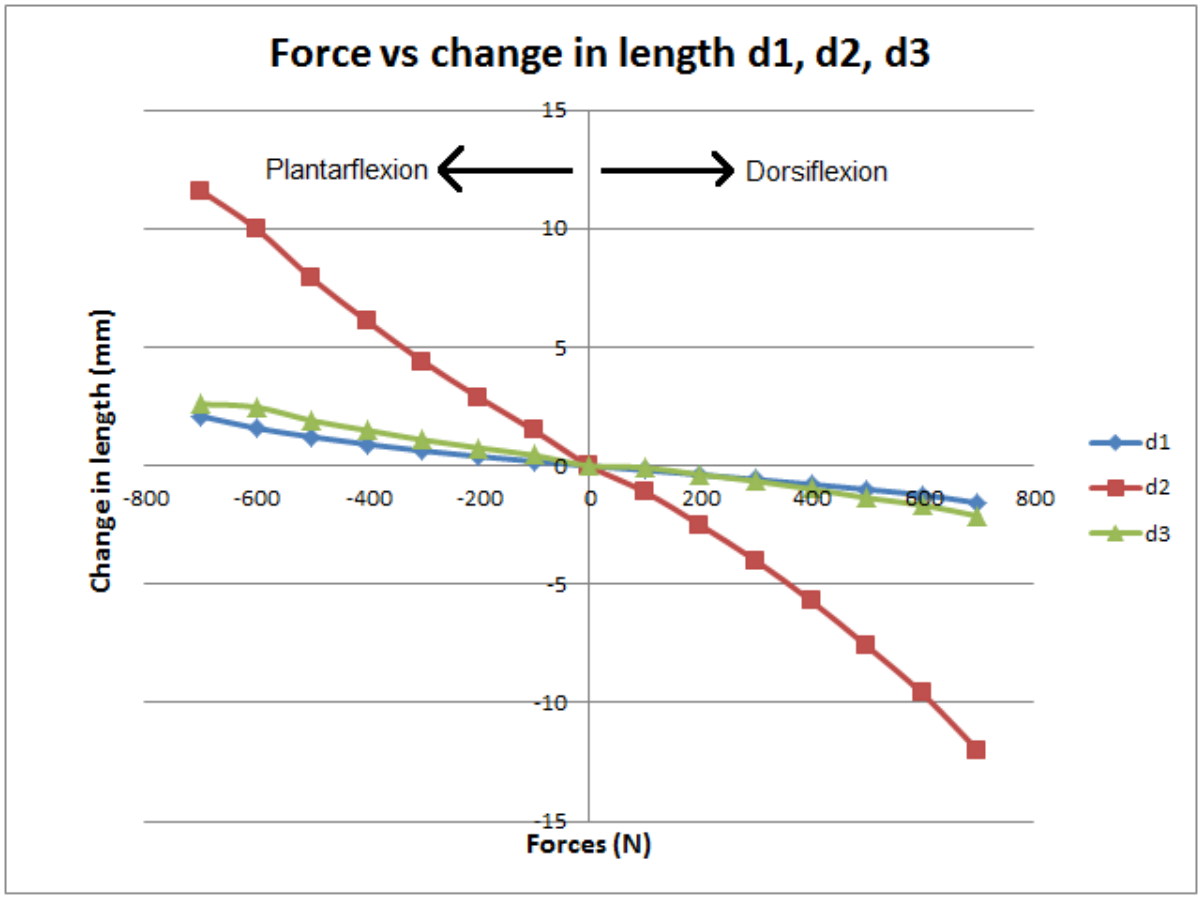

Figure 3.6 shows force (N) against change in length (mm) of d1, d2, d3. Positive forces corresponds to dorsiflexion and negative forces corresponds to plantarflexion.

We found d1, d2 and d3 to change with loading, although only d2 changes considerably higher than d1 and d3.

3.4 AFO stress distribution

The stress distribution was obtained from the post-processor function of Abaqus. This allows data collection of stresses over the whole AFO model. Stresses above 30MPa were ignored due ragged edges which appeared due limitations of the three-dimensional scanner (discussed later in chapter 4) especially at the circled region of the AFO (as seen in figure 3.7 and 3.8), thereby accumulation of high stress concentrations at those areas.

We found stress increasing with load and concentrated around the achilles tendon, circled region the AFO (as seen in figure 3.7 and 3.8), and at the interaction surface of steel rod and AFO. High stress concentration of around 20 - 22.5 MPa was seen at the ankle joint centre during dorsiflexion and plantarflexion under 700N and -700N respectively (figure 3.7 and 3.8). Appendix shows the distribution of stresses under all loads applied.

Our data also shows high point stress concentrations at contact point between the steel rod and the AFO model (see figure 3.7 and 3.8).

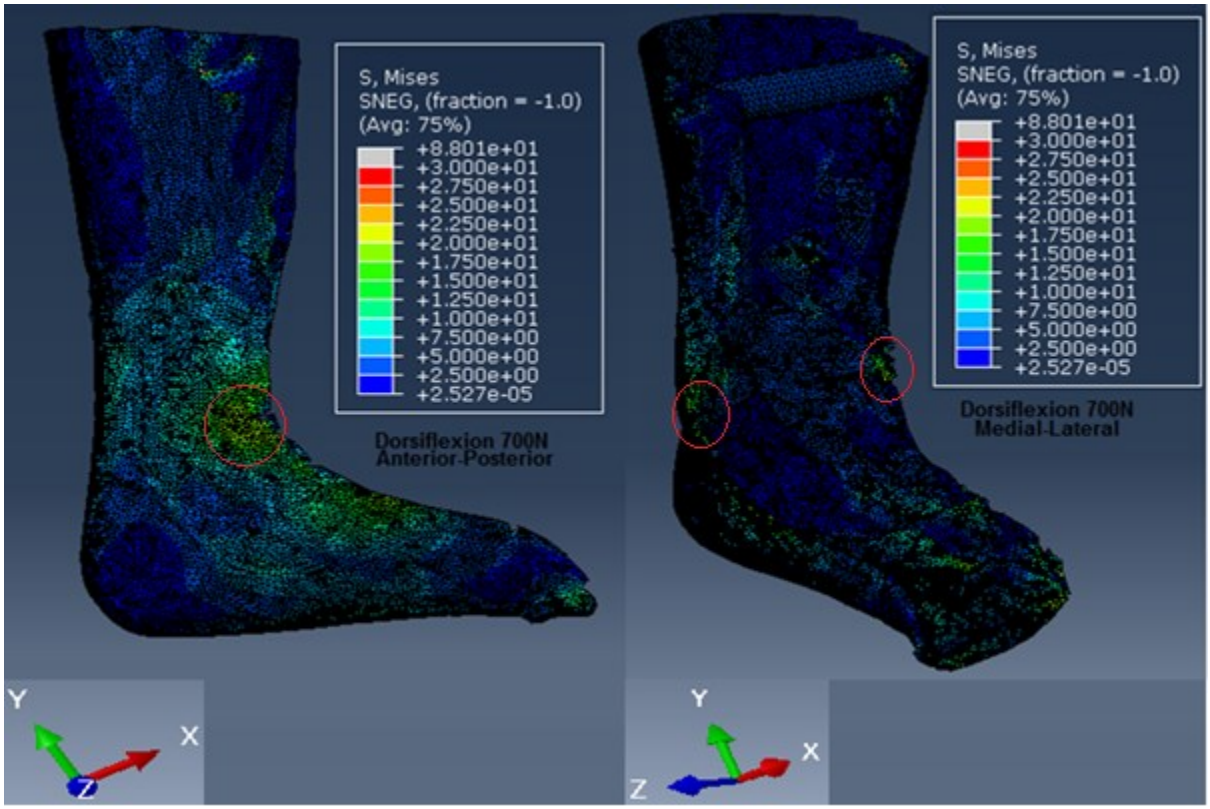

Figure 3.7 shows the anterior-posterior and medial-lateral view of the stress distribution of the AFO during dorsiflexion with 700N of force. Stresses are shown in colour bands. Each colour corresponds to specific range of stresses as shown in the figure Peak stresses are in the circled region.

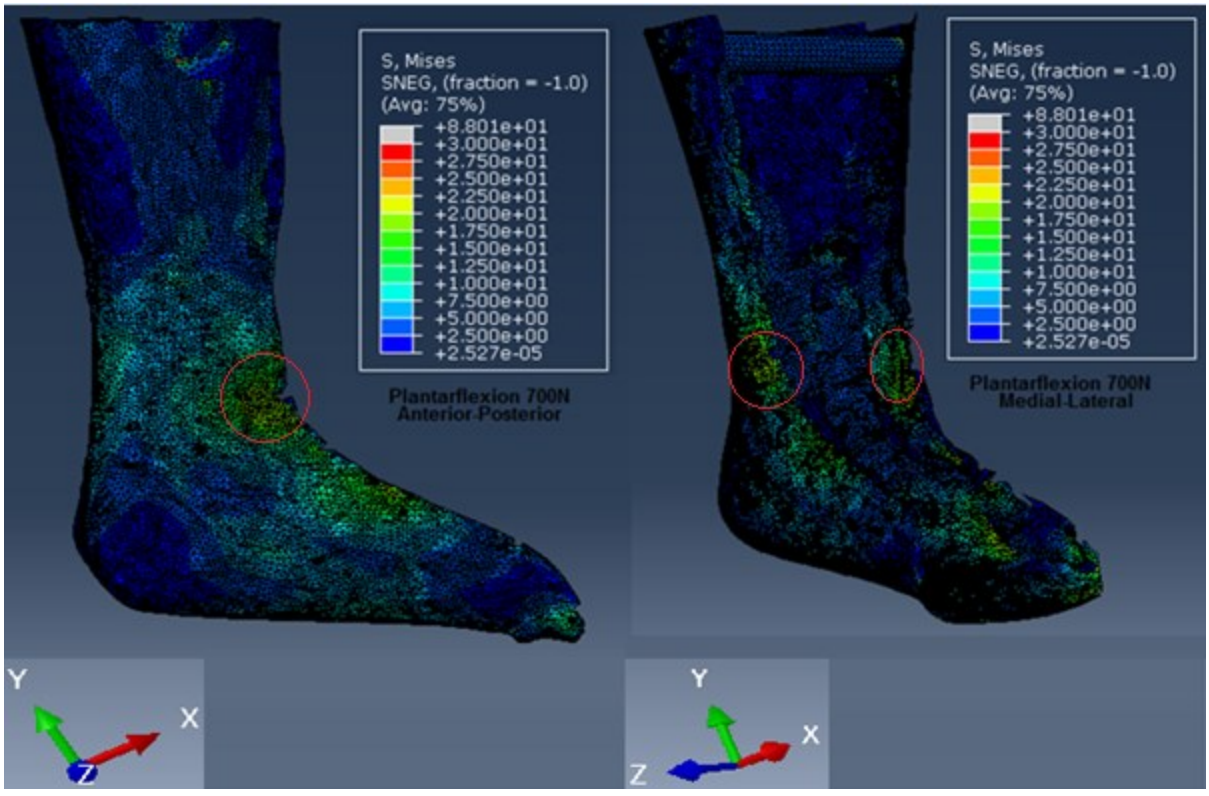

Figure 3.8 shows the anterior-posterior and medial-lateral view of the stress distribution of the AFO during plantarflexion with 700N of force. Stresses are shown in colour bands. Each colour corresponds to specific range of stresses as shown in the figure Peak stresses are in the circled region.

Chapter 4: Discussion

4.1 AFO stiffness

All experimental data (except one) available in literature have been conducted on co-polymer polypropylene AFOs. This makes comparison of our results to others difficult as there will be variations depending on the material, geometry, thickness and trimline differences. A study was conducted by Hagenbeek, 2013 on dorsiflexion and plantarflexion stiffness on co-polymer polypropylene with thickness of 4.6 mm. She found that during the initial stages (low load/stresses) the behaviour of the AFO was linear until approximately 25 Nm of moment and plantarflexion by 3.6°; but unfortunately we could not compare the non-linear region as data was not available (figure 4.1). During dorsiflexion, the change in ankle angle was 4.8° at 25 Nm (figure 4.2). This data suggests AFOs are stiffer during plantarflexion, as ours suggest this too.

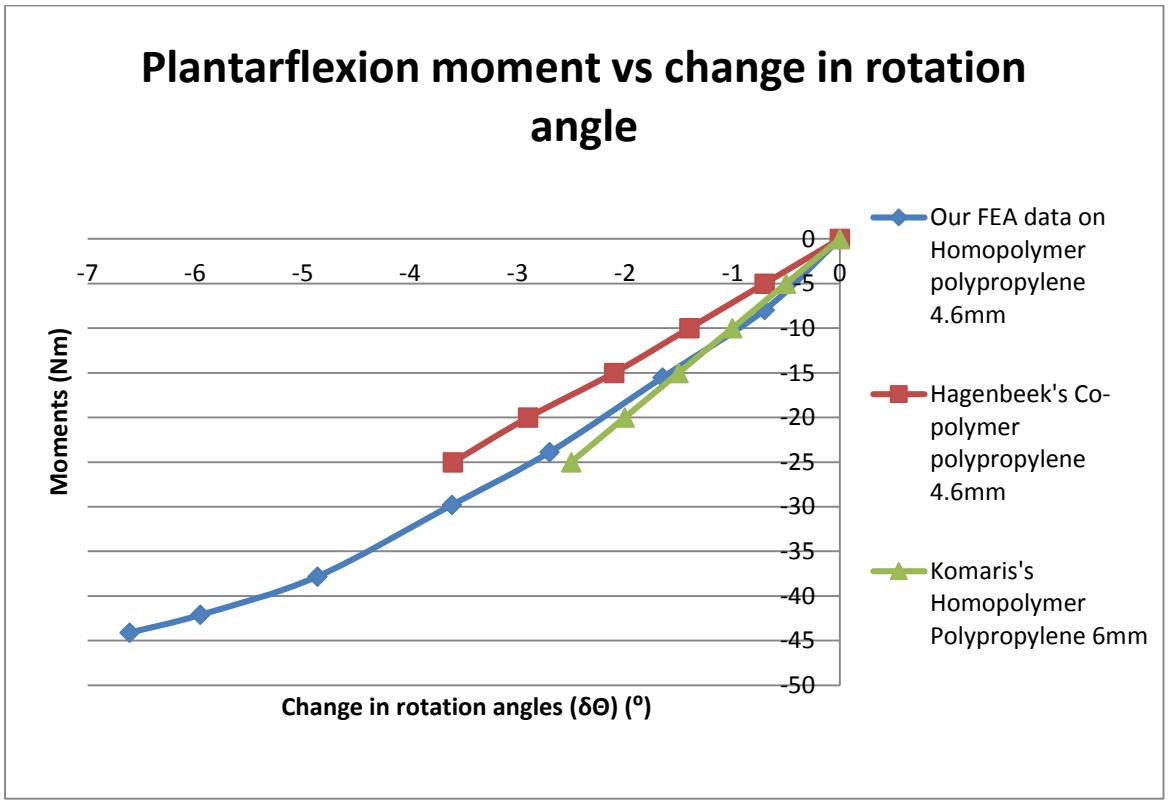

Figure 4.1 shows a graph for comparison of plantarflexion moment against change in ankle angle of our data, Hagenbeek's data (2013) and Komaris's data (2014)

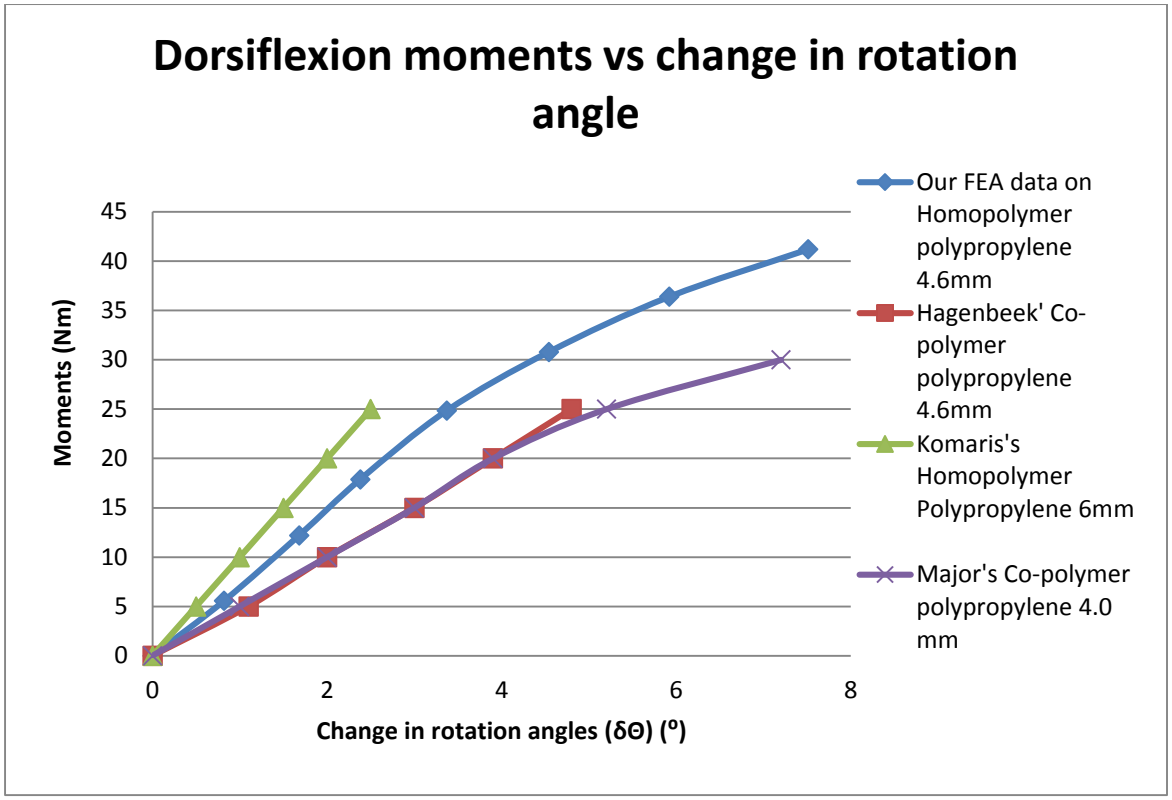

Figure 4.2 shows a graph for comparison of dorsiflexion moment against change in ankle angle of our data, Hagenbeek's data (2013), Komaris's data (2014) and Major's data (2004).

In 2004, a study conducted by Major et al, characterised the AFO response under dorsiflexion. They conducted the study on a 4 mm thick co-polymer polypropylene AFO, and found a linear region up to 10 Nm of moments and with 2.0° of dorsiflexion, above this point, the stiffness of the AFO and behave non-linearly. This result shows similar characteristics as our results by FEA. In comparison with Hagenbeek's 4.6mm thick AFO of the same material as Major's (i.e. copolymer polypropylene), both AFOs were seen to dorsiflex by the same amount of angle with response to the same moment. However we saw Hagenbeek's AFO responded linearly up to 25 Nm but Major's AFO started to decrease in stiffness above 10 Nm (figure 4.2).

The only experimental data with regard to stiffness testing found on homo-polymer polypropylene AFO with 6 mm thickness, was conducted by Komaris (2014). Komaris tested

the AFO in an Instron machine to investigate the stiffness during loading. He found linear region of the AFO response to be up to 20 Nm and 2.2° dorsiflexion and 22 Nm and 2.3° plantarflexion, above which, non-linear behaviour is seen. In comparison to our AFO, it was thicker by 1.4mm as such one would expect a higher stiffness compared to our model.

4.2 Buckling characteristics

The present results on buckling stress versus lateral displacements relationship at the malleoli represent the first investigation of its kind. As such results from our investigations may not be compared, subsequently may not be validated for its reliability. Thus this data cannot be compared with other publications.

However, Chu TM (1995) reporting on stress analysis of AFO, showed high stresses at the region of the malleoli (i.e. in the region of nodal point 22454 and 4254 the present model). It was also shown by Chu et al (1995) that AFOs are inherently geometrically asymmetrical and therefore peak stresses in medial and lateral surfaces are most likely to be different, as seen in our results as well. Chu presented the stress distribution but unfortunately did not specify the loading conditions applied to their model. Therefore, point to point comparison of stress values with the present work cannot be made.

We found the medial surface of the AFO model achieved a stress of 29.6 MPa which appears to be well above the yield as the stress steeply drops to 24 MPa (figure 3.4); this suggests the model had reached its yield point. The literature suggests homo-polymer type polypropylene material have a yield point of around 19 to 43 MPa dependant on chemical composition (Engineering and Design Plastics 2006, Plastics International 2004, P.K Mallick

et al 2003). Our results of 29.6 MPa does show some reliability as it is supported by available literature data on mechanical properties of polypropylene.

However, it is very likely our results on lateral displacements and buckling stresses may have errors caused by presence of ragged edges in the finite element model causing stress concentration effects. We were unable to improve on the ragged edges especially around the medial and lateral side arcs of the AFO model due to time constrains of this investigations and availability of a more accurate three-dimensional scanner.

4.3 Changes in lengths

Even in a prominent paper such as that of Major et al. (2004) it was assumed that the lengths d1 and d3 are constant under loading, and used as constant values d1 and d3 (see figure 1.6) for calculation of change in ankle angle using the cosine rule equation. We tried to verify this assumption as it seemed as an oversimplification of the AFO response to load.

Our results show that forces greatly affects length of d2 compared to d1 and d3, although we noted are some changes in d1 and d3 under load. Hence, all three lengths are affected by the loading. However, changes in lengths of d1 and d3 were seen to be minimal. This data suggests, Major's assumption on lengths of d1 and d3 under loading, is not entirely correct.

4.4 Stress distribution

The present results represent the first asymmetrical three-dimensional finite element model of an AFO as a non-linear material property. In the previous study on FEA on AFOs conducted by Chu et al. (1995), they used a linear elastic AFO model. They found that high stresses in AFOs under loading are concentrated around the malleoli, Achilles tendon and heel region. Our data is found to be consistent with Chu (1995), however we believe the peak stresses value of our model may contain errors.

We also found point peak stresses at the contact point of the AFO and the rod, this we believe is due to stress concentration at the contact point between the cylindrical rod and the AFO. This form of peak stresses is a classic phenomenon in *contact mechanics*. This is known has *Hertzian Theory of Deformation.* This theory describes the relation of circular contact areas of a sphere and cylinders with a plane.

Chapter 5: Conclusion and suggestion of further work

5.1 Sources of error

The finite element model was designed with material specification of previously investigated identical AFO. We also took careful considerations in all aspects of this finite element modelling, load and boundary conditions specification to simulate a stiffness testing of the AFO in a tensile testing machine (i.e. Instron machine); this was required in order to provide an accurate and reliable source of data.

A major source of error in this investigation is due to limitations of the three-dimensional scanner used. The AFO model had the following problems associated:

a) Ragged edges were seen, especially around the curvatures of AFO. The edges were sharp, instead of a smooth curve. This was due to the limitations of the three-dimensional scanner to capture images of the AFO with very high accuracy and precision. This may have led to higher stresses around that area, as stress will be concentrated at the cracks of the sharp edges leading to unreliable stress concentrations. In all our models we ignored stress concentrations above 30 MPa as high stress were concentrated at cracks of the sharp edge, as one would expect, which may mislead the results.

b) In an Instron machine, you would subject an AFO with a load at the middle of the steel rod and at the foot, and you would expect the force to travel through the medial and lateral surfaces of the AFO. In the FEA we conducted, we had a minor error with loading conditions in the AFO finite element model; where the load could not be placed on the middle of the steel rod due to problems with Abaqus unable to solve the mathematical analysis. In order to solve this issue, we placed the proximal

loads on the outer medial and lateral surface of the AFO, just below the steel rod edges (see figure 2.5).

These limitations could not be rectified due to time constraints on this investigations and availability of a three-dimensional scanner with higher accuracy and precision. Hence, careful consideration has to be taken in order to draw conclusions from these investigations.

5.2 Conclusion

Based on our investigations on FEA, we found that our characterisation of stiffness of a 4.6 mm homopolymer polypropylene AFO compared well with other data in the literature. The location of the dorsiflexion and plantarflexion curves of our model (see figure 4.1 and 4.2) are as one would expect for the particular AFO analysed. This shows FEA that the model is reliable and accurate in terms of predicting stiffness of an AFO.

The stress distribution in our results concludes that high stresses were concentrated at the malleoli, and Achilles tendon region on the AFO. This result is similar to Chu et al. 1995, however we may not compare the value of the peak stress at these authors did not specify the loads. This shows FEA is reliable in predicting stress distribution but further works needs to be done to prepare an accurate finite element model of an AFO, and to compare with experimental data on AFOs using strain gauges to validate the accuracy of FEA.

Major et al (2004) was first to introduce the cosine rule in calculation of change in lengths of shank, foot and proximal to distal force points (i.e. completing a triangle of an AFO) of the AFO. In their calculation they assumed the lengths of shank and foot of the AFO to be constant. Based on our data, we showed both shank and foot lengths change with loading, although only minimally. Therefore, their assumption does not hold.

Overall we conclude FEA is a reliable computational method in predicting mechanical characteristics and stress distributions, although we may not conclude on accuracy of particular values of stresses.

5.3 Further work

There were some shortcomings in our investigations; as such we should conduct further work to rectify those sources of error.

As we saw some problems with ragged edges of the AFO scanned sections and conducted our investigation on an inaccurate AFO model, we should in future, re-scan the AFO to achieve an accurate finite element model. This includes proper stitching and smoothening of any surface problems or ragged edges we may find. This may be done by using computer software to process three-dimensional images for the purpose of designing and modelling, such as *Mimics* (Materialise NV, Belgium). Also, to conduct all the investigations again, ensure reliability and accuracy can be validated.

In our investigation, we simulated the loading of an AFO in an Instron machine, where the load travels from the steel rod and is transferred to the body of the AFO. This is not what occurs in real life on a patient. In a patient, the load travels through the lower leg of the patient to the foot of the AFO. In future analysis, we should try to improve the finite element model of the AFO in including the shank, foot and to assign material properties of bones, ligaments, soft tissue and orthosis to them. We need to pay close attention to loading and boundary conditions of the model as well, and to use functional data of AFOs during patient's gait. This will ensure that the investigation will simulate what occurs in real life in a patient.

References

3D System Inc. Geomagic (http://www.rapidform.com/3d-scanners/) 2008

ABAQUS USER MANUAL, Dassault Systemes Ltd, 2012

Advanced Orthotic Design Inc. (http://www.aodmobility.com/custom-devices/AFO/) 2004

Al Hasan. S, Lower Limb Orthoses: A Review, JCMCTA 2008; 19 (1) 33-36

Bregman, D.J.J., Rozumalski, A., Koops, D., de Groot, V., Schartz, M., Harlaar, J. A new method for evaluating ankle foot orthosis characteristics: BRUCE. Gait & Posture. 2009; 30(2): 144-149.

Chu TM, Reddy NP, Three-dimensional finite element stress analysis of the polypropylene, ankle-foot orthosis: static analysis, Medical Engineering Physics, Elsevier Science, 1995, Vol 17, 5, 372-379

Chu TM, Gent AN, Reddy NP, Bonding Methods for Strain Gauge on Polypropylene material. Experimental Techniques, 1996, 20 (5):29

Chu TM, Feng R, Determination of Stress Disribution in various ankle foot orthoses: Experimental Stress Analysis. Journal of Prosthetics and Orthotics, 1998 10 (1):11-16.

Chu TM, Determination of peak stress on polypropylene ankle-foot orthoses due to weight change using strain gauge technology. Experimental Techniques, 2000 24(2)28-30.

Chu TM, Biomechanics of Ankle-foot Orthoses: Past, Present and Future, Topics in Stroke Rehabilitation, 2001, 7(4): 19-28

Engineering & Design Plastics Ltd, (http://www.edplastics.co.uk/Polypropylene.htm)

Hagenback J, The direct effects of variations in AFO stiffness on the kinematics and kinetics of gait, MSc thesis, University of Strathclyde, 2013.

Kobayashi, T., Leung, A.K.L., Hutchins, S.W. Techniques to measure rigidity of ankle-foot orthosis: A review. Journal of Rehabilitation Research and Development. 2011; 48(5): 565-576.

Kobayashi, T., Leung, A.K.L., Akazawa, Y., Naito, H., Hutchins, S.W. Design of an automated device to measure sagittal plane stiffness of an articulated ankle-foot orthosis. Prosthetics and Orthotics International. 2010; 34(4): 439-348.

Komaris DS, Investigation of bench method for determining stiffness of solid ankle foot orthoses, MSc thesis, University of Strathclyde, 2014.

Lam PC, Downing M, One more step in redesigning the ankle-foot orthosis, SOMA 1987, 2:36-7

Leone DJ, A structural model for molded thermoplastic ankle-foot orthoses. J Biomech Engineering, 1987; 109: 305-10.

Leone DJ, Diemente S, Structural analysis of solid ankle-foot orthosis. Proceedings of the 14th Annual Northeast Bioegineering Conference 1988, 26-8

Leone D, Diemente S, Structural stability predicion for thermoplastic ankle-foot orthoses. Proceedings of the 1991, IEEE, 17th Annual Northeast Biengineering Conference, 1991: 231-2

Lehmann JF, Biomechanics of ankle foot orthoses prescription and design. Archives of Physical Medicine and Rehabilition 60:200-207

Lehneis, H.R., Frisina, W., Marx, H.W., Sowell, T.T. Bioengineering design and development of lower-extremity orthotic devices. Bulletin of Prosthetics Research. 1973; 10(20), 132-202

Martini F, Fundamentals of Anatomy and Physiology, 7th edition, Pearson, 2006.

Major RE, Heward PJ, A new structural concept in moulded fixed ankle foot orthoses and comparison of the bending stiffness of four constructions,Prosthetics and orthotics International, 2004, 28: 44

Miyazaki, S., Yamamoto, S., Kubota, T. Effect of ankle-foot orthosis on active ankle moment in patient with hemiparesis. Medical & Biological Engineering & Computing. 1997; 60: 381-385

Nordin, M., Frankel, V.H. Basic Biomechanics of the Musculoskeletal System. Third edition. Philadelphia: Lippincott Williams & Wilkins; 2001

Ottobock. (http://professionals.ottobockus.com) 2008

Orthomedics (http://www.orthomedics.us/Pages/ankle.aspx)

P.K Mallick, Yuanxin Zhuo, yield and fatigue behaviour of polypropylene and polyamide-6 nanocomposite, Journal of Materials Science (2003) 3183-3190.

Payne C, Position of the subtalar joint axis and resistance of the rearfoot to supination, J Am Podiatr Med Assoc. 2003 Mar-Apr;93(2):131-5.

Papi E, Investigate the use of strain gauge technology for the determination of the mechanical characteristics of polypropylene ankle-foot orthosis, MSc Thesis at University of Strathclyde, 2008.

Papi E, An investigation of the methodologies for biomechanical assessment of stroke rehabilitation, PhD thesis at University of Strathclyde, 2012.

Perry, J., Burnfield, J.M. Gait analysis. Normal and Pathological Function. Second edition. Thorofare: SLACK Incorporated; 201

Plastics International, Polypropylene Homopolymer Characteristics, (https://www.plasticsintl.com/datasheets/Polypropylene_Homopolymer.pdf)

Reddy NP, Pohit G Lam PC, Finite element modelling of Ankle-foot Orthoses. Proc Inter Conf Biomechanics and Clinical Kinesiology of Hand and Foot, IIT, 1985, 97-9

Solomonidis.S , Foot and Akle deformities Ankle foot orthoses (AFOs), Biomedical Engineering, November 2007.

Showers David C,Sheet Plastics and their application in Orthotics and Prosthetics. Orthotics and Prosthetics, 1985, 38(4): 41-48

Sumiya T, Suzuki Y, Stiffness control in posterior-type plastic ankle-foot orthoses: effect of ankle trimline. Part 2. Orthosis characteristics and orthosis/patient matching, Prosthetic and Orthotics International 1996, 20:132-7

Syngellakis S, MA Arnold, H Rassoulian, Assessment of the non-linear behaviour of plastic ankle foot orthoses by the finite element method, Proceedings of the Institution of Mechanical Engineers, Part H: Journal of Engineering in Medicine, 2000, 214:527

Truelson T et al, The global burden of cerebrovascular disease, Global Burden of Disease 2000.

World Health Organization MONICA Project (Monitoring trends and determinants in cardiovascular disease). J Clin Epidemiol 41, 2000, 105-114.

Yamamoto, S., Kubo, S., Ebina, M., Hayashi, T., Iwasak, M., Kawai, H. Quantification of the effect of dorsi-/plantarflexibility of ankle-foot orthoses on hemiplegic gait:A preliminary report. JPO: Journal of Prosthetics and Orthotics. 1993b; 5(3): 42-48.

Yamamoto, S., Kubo, S., Ebina, M., Hayashi, T., Iwasak, M., Kawai, H. Quantification of the effect of dorsi-/plantarflexibility of ankle-foot orthoses on hemiplegic gait: A preliminary report. JPO: Journal of Prosthetics and Orthotics. 1993b; 5(3): 42-48.

Chapter 6: Appendix

Calculation method of change in ankle angles (δθ)

Coordinates of nodal points 23338 (A), 9868 (B), 16185 (C).

Equation used $\boldsymbol{a} \cdot \boldsymbol{b} = |\boldsymbol{a}||\boldsymbol{b}| \cos\boldsymbol{\theta}$ **where a = position vector of A with respect to B, where b = position vector of C with respect to B and θ = angle of ABC.**

Step 1 : given will be the two vectors of the form:

$A = a_1 i + b_1 j + c_1 k$

$B = a_2 i + b_2 j + c_2 k$

where a_1, b_1, c_1 and a_2, b_2, c_2 are the components of A and B.

Step 2 : Calculate the value of |A| and |B| given as:

$$|A| = \sqrt{a_1^2 + b_1^2 + c_1^2}$$

$$|B| = \sqrt{a_2^2 + b_2^2 + c_2^2}$$

Step 3 : Then using the below formula, calculate the value of cos θ

$$\cos\theta = \frac{a_1a_2 + b_1b_2 + c_1c_2}{|A||B|}$$

and from that get the value of θ using formula:

$$\theta = \cos^{-1}\frac{a_1a_2 + b_1b_2 + c_1c_2}{|A||B|}$$

which gives the answer.

Figure 6.1 shows calculation steps to calculate the ankle angles from nodal point coordinates

Coordinates of deformed and undeformed points

Undeformed Coordinates		
	X	Y
A	18.18	136.8
B	-46.11	-6.278
C	16.31	-130.4

Deformed Coordinates		
100N	X	Y
A	18.18	136.8
B	-46.96	-5.69
C	16.31	-129.3

Deformed Coordinates		
-100	X	Y
A	18.18	136.8
B	-45.27	-6.86
C	16.31	-131.9

Deformed Coordinates		
200N	X	Y
A	18.18	136.8
B	-47.84	-5.08
C	16.31	-127.9

Deformed Coordinates		
-200	X	Y
A	18.18	136.8
B	-44.38	-7.48
C	16.31	-133.3

Deformed Coordinates		
300N	X	Y
A	18.18	136.8
B	-48.81	-4.4
C	16.31	-126.4

Deformed Coordinates		
-300	X	Y
A	18.18	136.8
B	-43.41	-8.15
C	16.31	-134.8

Deformed Coordinates		
400N	X	Y
A	18.18	136.8
B	-49.88	-3.66
C	16.31	-124.7

Deformed Coordinates		
-400	X	Y
A	18.18	136.8
B	-42.34	-8.9
C	16.31	-136.5

Deformed Coordinates		
500N	X	Y
A	18.18	136.8
B	-51.06	-2.84
C	16.31	-122.8

Deformed Coordinates		
-500	X	Y
A	18.18	136.8
B	-41.16	-9.72
C	16.31	-138.3

Deformed Coordinates		
600N	X	Y
A	18.18	136.8
B	-52.36	-1.93
C	16.31	-120.8

Deformed Coordinates		
-600	X	Y
A	18.18	136.8
B	-39.87	-10.63
C	16.31	-140.4

Deformed Coordinates		
700N	X	Y
A	18.18	136.8
B	-53.71	-0.853
C	16.31	-118.4

Deformed Coordinates		
-700	X	Y
A	18.18	136.8
B	-38.51	-11.7
C	16.31	-140.3

Dorsiflexion Load		Plantarflexion Load	
Degrees (°)	Moments (Nm)	Degrees (°)	Moments (Nm)
0.82	5.56	-0.7	-7.96
1.68	12.2	-1.65	-15.51
2.38	17.88	-2.7	-23.88
3.37	24.84	-3.61	-29.8
4.54	30.8	-4.86	-37.8
5.92	36.4	-5.95	-42.1
7.51	41.2	-6.61	-44.1

Table 2 shows the values of moments and corresponding change in ankle angle.

	change in d1 (mm)	change in d2 (mm)	change in d3 (mm)
700	-1.563353176	-12.0001488	-2.112592285
600	-1.224420334	-9.600212628	-1.654555799
500	-0.994554376	-7.600264918	-1.350866949
400	-0.777631114	-5.700313852	-0.978218316
300	-0.572983671	-4.000357037	-0.642227287
200	-0.370042294	-2.50039468	-0.370025966
100	-0.184691182	-1.100429431	-0.07246825
0	0	0	0
-100	0.18977576	1.499506992	0.447124978
-200	0.40095092	2.899473266	0.758335151
-300	0.634019178	4.399437516	1.089929741
-400	0.91102655	6.099397474	1.499551903
-500	1.221888512	7.899355615	1.904976494
-600	1.588559862	9.999307468	2.474787916
-700	2.094542378	11.599309744	2.592968494

Table 3 shows the calculated results for change in lengths for d1,d2,d3.

AFO stress distribution under load during dorsiflexion and plantarflexion

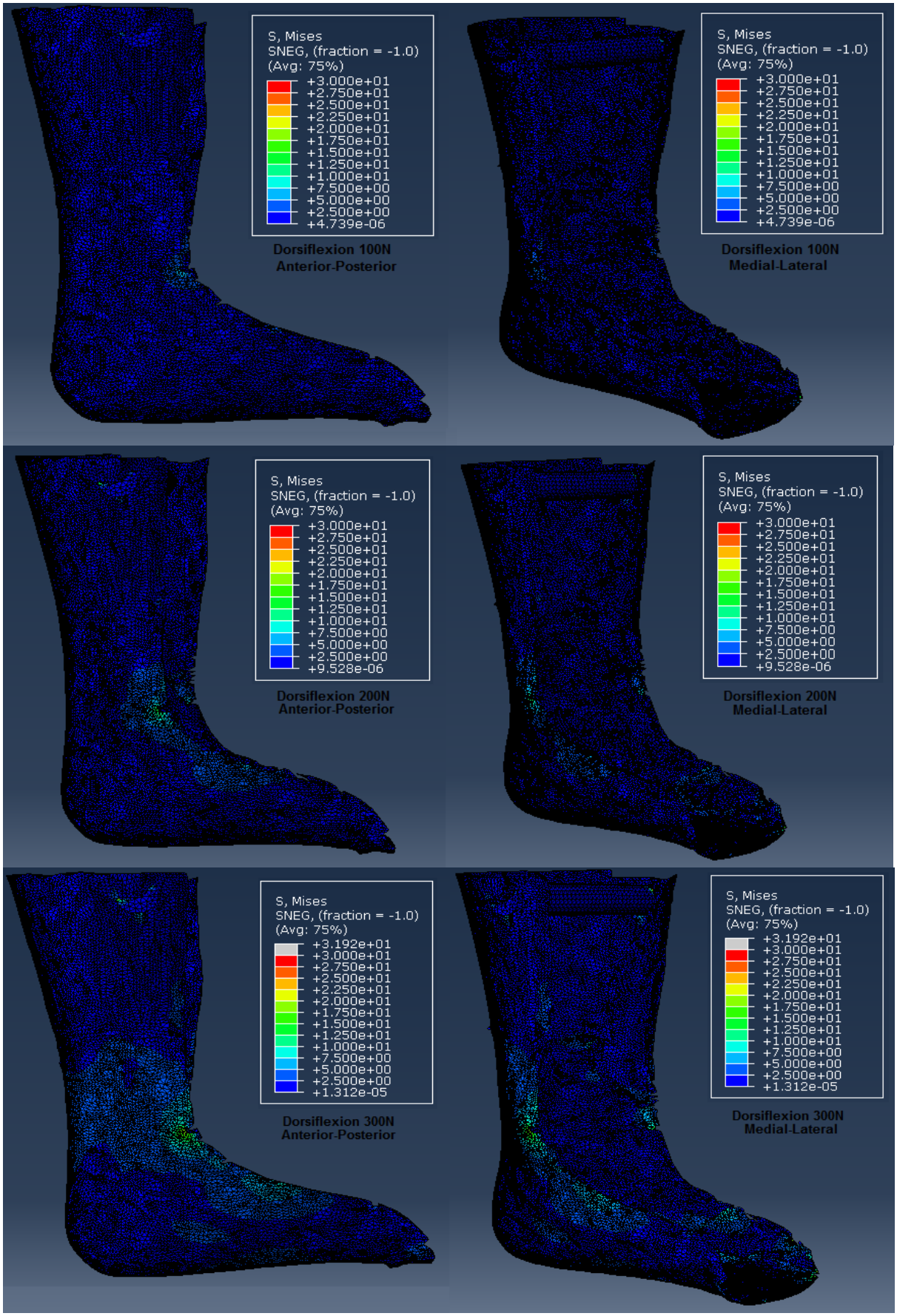

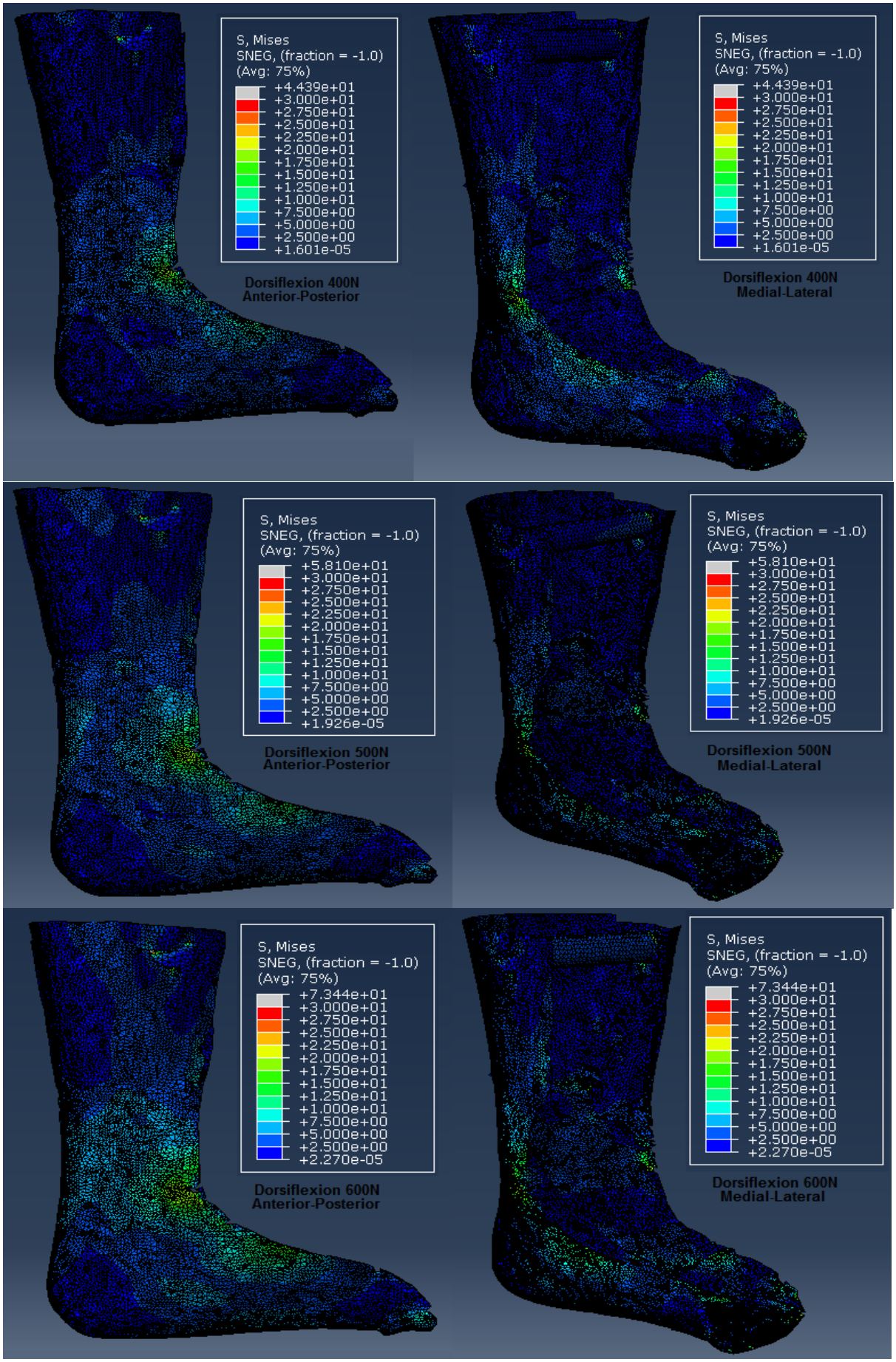
S, Mises
SNEG, (fraction = -1.0)
(Avg: 75%)
+4.439e+01
+3.000e+01
+2.750e+01
+2.500e+01
+2.250e+01
+2.000e+01
+1.750e+01
+1.500e+01
+1.250e+01
+1.000e+01
+7.500e+00
+5.000e+00
+2.500e+00
+1.601e-05
Dorsiflexion 400N
Anterior-Posterior
S, Mises
SNEG, (fraction = -1.0)
(Avg: 75%)
+4.439e+01
+3.000e+01
+2.750e+01
+2.500e+01
+2.250e+01
+2.000e+01
+1.750e+01
+1.500e+01
+1.250e+01
+1.000e+01
+7.500e+00
+5.000e+00
+2.500e+00
+1.601e-05
Dorsiflexion 400N
Medial-Lateral
S, Mises
SNEG, (fraction = -1.0)
(Avg: 75%)
+5.810e+01
+3.000e+01
+2.750e+01
+2.500e+01
+2.250e+01
+2.000e+01
+1.750e+01
+1.500e+01
+1.250e+01
+1.000e+01
+7.500e+00
+5.000e+00
+2.500e+00
+1.926e-05
Dorsiflexion 500N
Anterior-Posterior
S, Mises
SNEG, (fraction = -1.0)
(Avg: 75%)
+5.810e+01
+3.000e+01
+2.750e+01
+2.500e+01
+2.250e+01
+2.000e+01
+1.750e+01
+1.500e+01
+1.250e+01
+1.000e+01
+7.500e+00
+5.000e+00
+2.500e+00
+1.926e-05
Dorsiflexion 500N
Medial-Lateral
S, Mises
SNEG, (fraction = -1.0)
(Avg: 75%)
+7.344e+01
+3.000e+01
+2.750e+01
+2.500e+01
+2.250e+01
+2.000e+01
+1.750e+01
+1.500e+01
+1.250e+01
+1.000e+01
+7.500e+00
+5.000e+00
+2.500e+00
+2.270e-05
Dorsiflexion 600N
Anterior-Posterior
S, Mises
SNEG, (fraction = -1.0)
(Avg: 75%)
+7.344e+01
+3.000e+01
+2.750e+01
+2.500e+01
+2.250e+01
+2.000e+01
+1.750e+01
+1.500e+01
+1.250e+01
+1.000e+01
+7.500e+00
+5.000e+00
+2.500e+00
+2.270e-05
Dorsiflexion 600N
Medial-Lateral

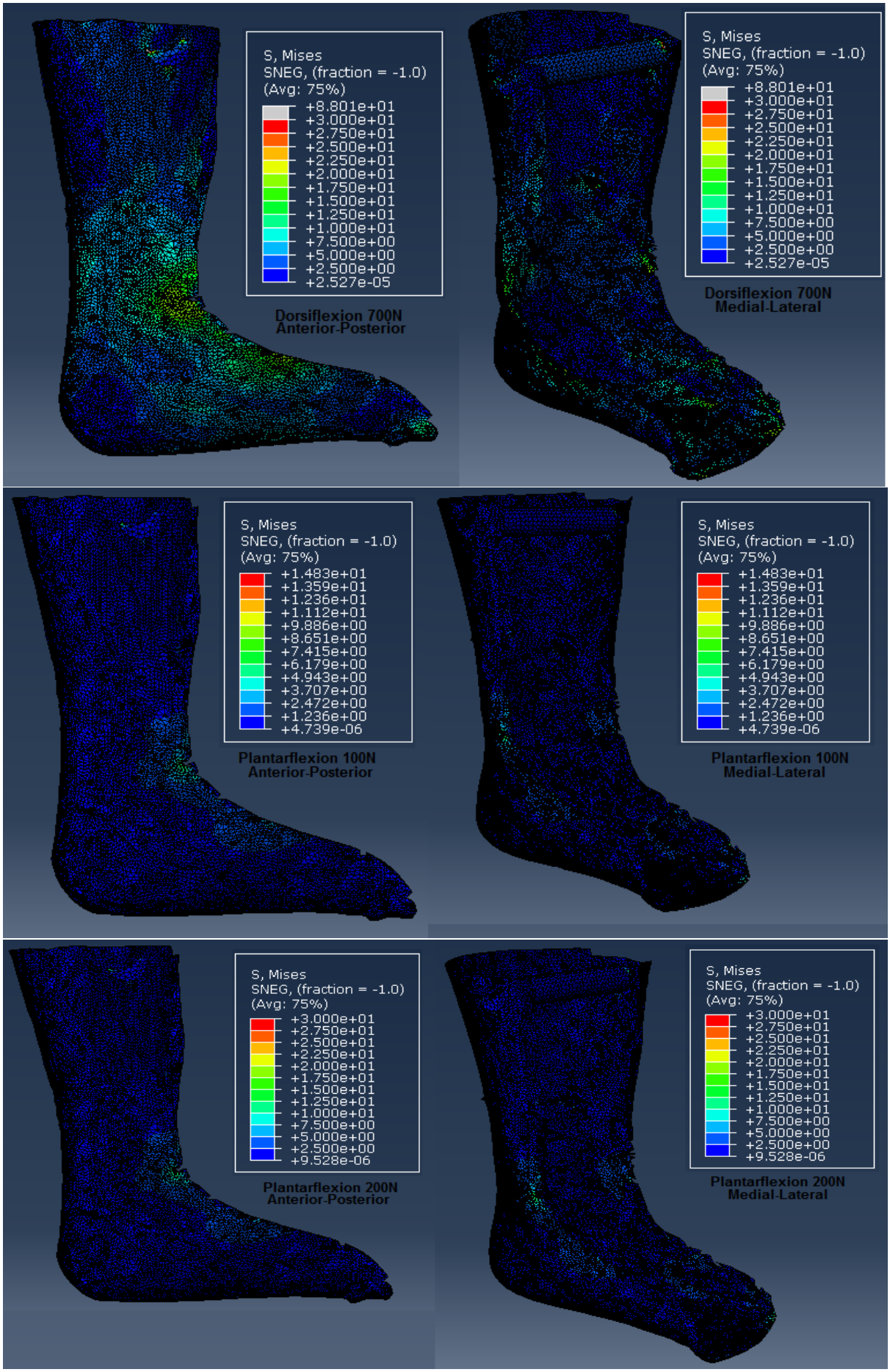
S, Mises
SNEG, (fraction = -1.0)
(Avg: 75%)
+8.801e+01
+3.000e+01
+2.750e+01
+2.500e+01
+2.250e+01
+2.000e+01
+1.750e+01
+1.500e+01
+1.250e+01
+1.000e+01
+7.500e+00
+5.000e+00
+2.500e+00
+2.527e-05
Dorsiflexion 700N
Anterior-Posterior
S, Mises
SNEG, (fraction = -1.0)
(Avg: 75%)
+8.801e+01
+3.000e+01
+2.750e+01
+2.500e+01
+2.250e+01
+2.000e+01
+1.750e+01
+1.500e+01
+1.250e+01
+1.000e+01
+7.500e+00
+5.000e+00
+2.500e+00
+2.527e-05
Dorsiflexion 700N
Medial-Lateral
S, Mises
SNEG, (fraction = -1.0)
(Avg: 75%)
+1.483e+01
+1.359e+01
+1.236e+01
+1.112e+01
+9.886e+00
+8.651e+00
+7.415e+00
+6.179e+00
+4.943e+00
+3.707e+00
+2.472e+00
+1.236e+00
+4.739e-06
Plantarflexion 100N
Anterior-Posterior
S, Mises
SNEG, (fraction = -1.0)
(Avg: 75%)
+1.483e+01
+1.359e+01
+1.236e+01
+1.112e+01
+9.886e+00
+8.651e+00
+7.415e+00
+6.179e+00
+4.943e+00
+3.707e+00
+2.472e+00
+1.236e+00
+4.739e-06
Plantarflexion 100N
Medial-Lateral
S, Mises
SNEG, (fraction = -1.0)
(Avg: 75%)
+3.000e+01
+2.750e+01
+2.500e+01
+2.250e+01
+2.000e+01
+1.750e+01
+1.500e+01
+1.250e+01
+1.000e+01
+7.500e+00
+5.000e+00
+2.500e+00
+9.528e-06
Plantarflexion 200N
Anterior-Posterior
S, Mises
SNEG, (fraction = -1.0)
(Avg: 75%)
+3.000e+01
+2.750e+01
+2.500e+01
+2.250e+01
+2.000e+01
+1.750e+01
+1.500e+01
+1.250e+01
+1.000e+01
+7.500e+00
+5.000e+00
+2.500e+00
+9.528e-06
Plantarflexion 200N
Medial-Lateral

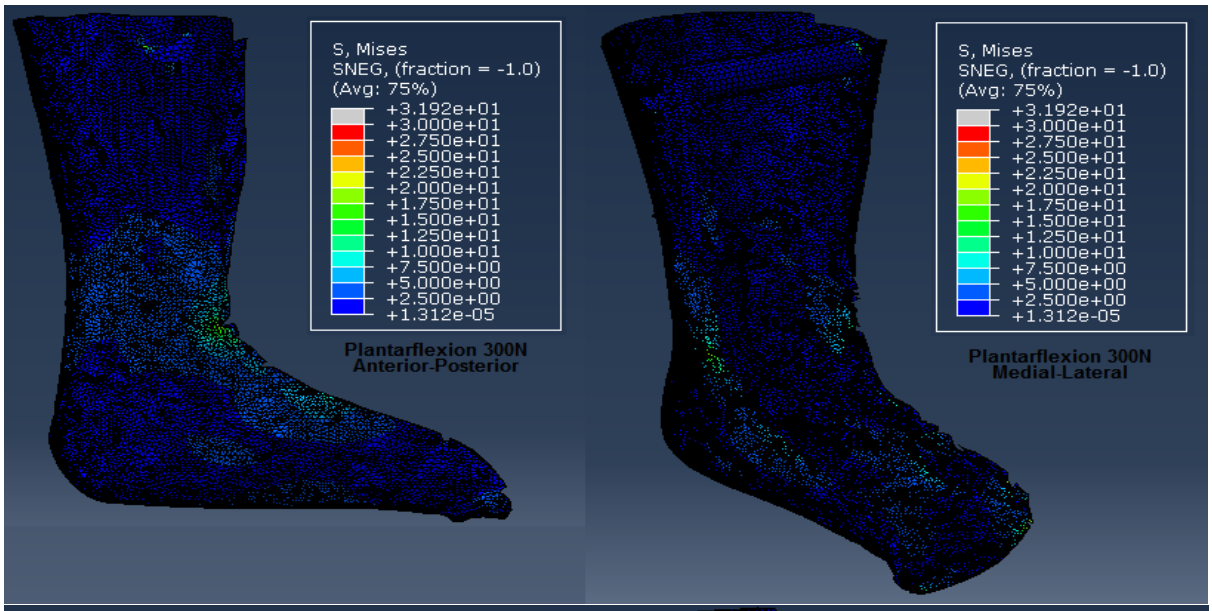
S, Mises
SNEG, (fraction = -1.0)
(Avg: 75%)
+3.192e+01
+3.000e+01
+2.750e+01
+2.500e+01
+2.250e+01
+2.000e+01
+1.750e+01
+1.500e+01
+1.250e+01
+1.000e+01
+7.500e+00
+5.000e+00
+2.500e+00
+1.312e-05
Plantarflexion 300N
Anterior-Posterior
S, Mises
SNEG, (fraction = -1.0)
(Avg: 75%)
+3.192e+01
+3.000e+01
+2.750e+01
+2.500e+01
+2.250e+01
+2.000e+01
+1.750e+01
+1.500e+01
+1.250e+01
+1.000e+01
+7.500e+00
+5.000e+00
+2.500e+00
+1.312e-05
Plantarflexion 300N
Medial-Lateral

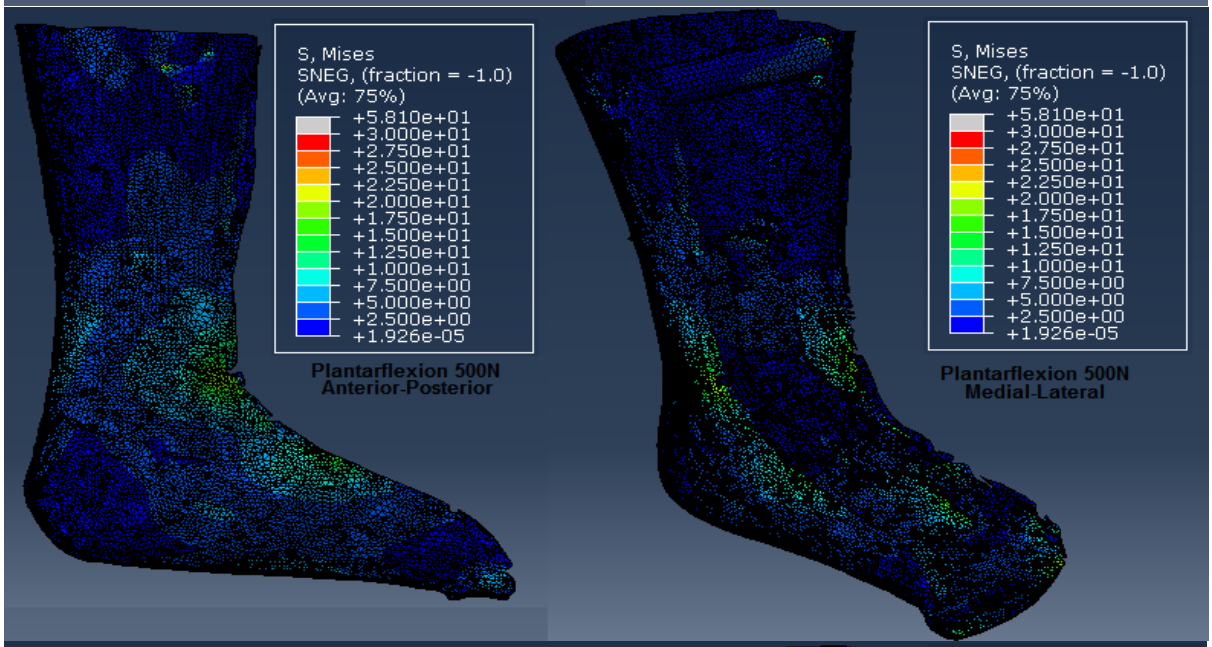
S, Mises
SNEG, (fraction = -1.0)
(Avg: 75%)
+5.810e+01
+3.000e+01
+2.750e+01
+2.500e+01
+2.250e+01
+2.000e+01
+1.750e+01
+1.500e+01
+1.250e+01
+1.000e+01
+7.500e+00
+5.000e+00
+2.500e+00
+1.926e-05
Plantarflexion 500N
Anterior-Posterior
S, Mises
SNEG, (fraction = -1.0)
(Avg: 75%)
+5.810e+01
+3.000e+01
+2.750e+01
+2.500e+01
+2.250e+01
+2.000e+01
+1.750e+01
+1.500e+01
+1.250e+01
+1.000e+01
+7.500e+00
+5.000e+00
+2.500e+00
+1.926e-05
Plantarflexion 500N
Medial-Lateral

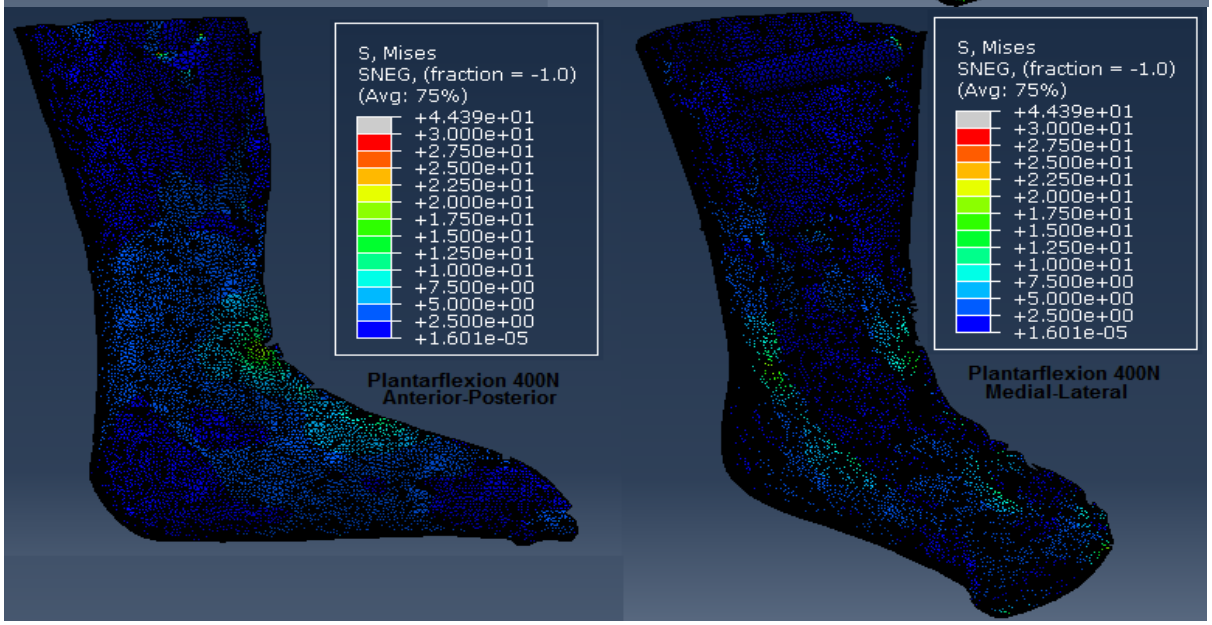
S, Mises
SNEG, (fraction = -1.0)
(Avg: 75%)
+4.439e+01
+3.000e+01
+2.750e+01
+2.500e+01
+2.250e+01
+2.000e+01
+1.750e+01
+1.500e+01
+1.250e+01
+1.000e+01
+7.500e+00
+5.000e+00
+2.500e+00
+1.601e-05
Plantarflexion 400N
Anterior-Posterior
S, Mises
SNEG, (fraction = -1.0)
(Avg: 75%)
+4.439e+01
+3.000e+01
+2.750e+01
+2.500e+01
+2.250e+01
+2.000e+01
+1.750e+01
+1.500e+01
+1.250e+01
+1.000e+01
+7.500e+00
+5.000e+00
+2.500e+00
+1.601e-05
Plantarflexion 400N
Medial-Lateral

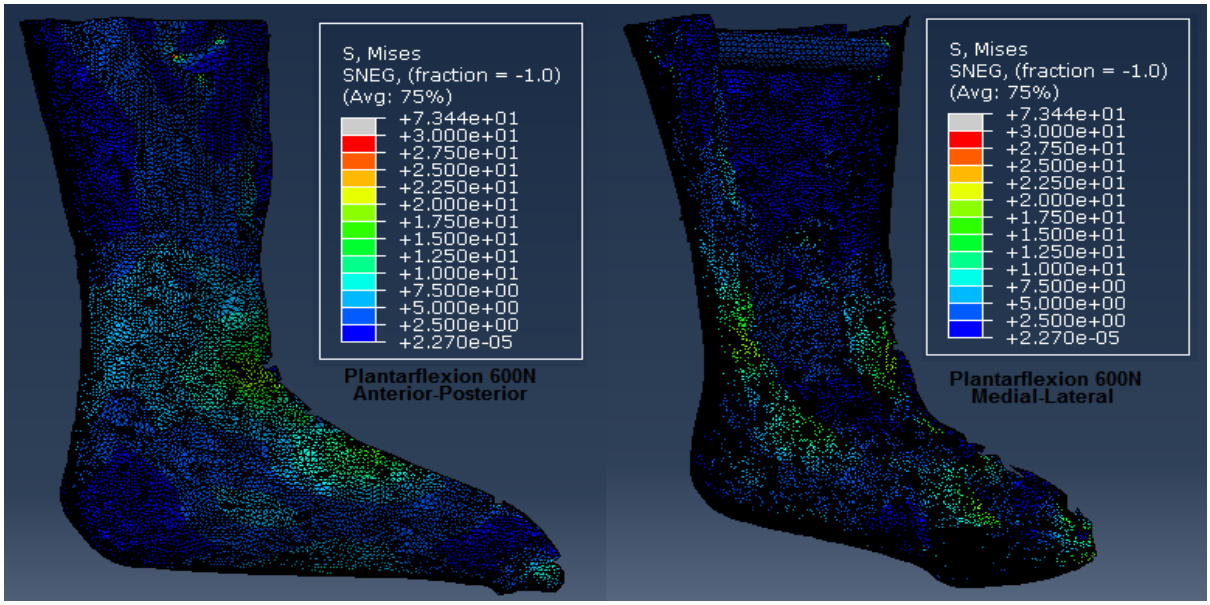
S, Mises
SNEG, (fraction = -1.0)
(Avg: 75%)
+7.344e+01
+3.000e+01
+2.750e+01
+2.500e+01
+2.250e+01
+2.000e+01
+1.750e+01
+1.500e+01
+1.250e+01
+1.000e+01
+7.500e+00
+5.000e+00
+2.500e+00
+2.270e-05
Plantarflexion 600N
Anterior-Posterior
S, Mises
SNEG, (fraction = -1.0)
(Avg: 75%)
+7.344e+01
+3.000e+01
+2.750e+01
+2.500e+01
+2.250e+01
+2.000e+01
+1.750e+01
+1.500e+01
+1.250e+01
+1.000e+01
+7.500e+00
+5.000e+00
+2.500e+00
+2.270e-05
Plantarflexion 600N
Medial-Lateral